12 Negative-Ion Formation Processes and Sources

G.D. Alton

Physics Division, Oak Ridge National Laboratory**, Oak Ridge, Tennessee 37831-6368, USA
gda@ornl.gov

12.1 Introduction

Most elements and many molecules form stable negative ions by adding an electron to the neutral atom or molecule. The existence of the negative-ion state has provided an additional means for producing charged beams. Negative ions can be formed through several processes. In this chapter, particular emphasis is placed on high-probability negative-ion formation processes of dissociative attachment, charge transfer, thermodynamic-equilibrium surface ionization and nonthermodynamic secondary-ion formation processes, and negative-ion sources. Early treatises devoted to the negative-ion state have been written by Massey [1] and Smirnov [2]. Many experimental measurements and theoretical predictions have been made of electron affinities (binding energies) of elements [3–20], as well as for electronegative molecules [21–33]. In addition, multiple electrons can be attached to certain complex-structure molecules; this subject has been reviewed [34].

Negative-ion beams have been used for many years in fundamental accelerator-based physics, as well as in applied research. As an example, H^- beams have been used as sources of neutral beams for heating plasmas by injection into controlled thermonuclear-plasma-fusion research devices. The applications have provided the impetus for the development of sources capable of producing negative ion beams containing almost every element. Sources generally are characterized by the mechanism utilized for production of negative ions (e.g. volume production in plasmas, charge exchange, thermodynamic-equilibrium surface ionization and nonthermodynamic secondary surface ionization phenomena). In certain cases, two or more mechanisms may be involved in the production process. The sources vary in operational and mechanical complexity, depending on the method required to produce the desired ion species and beam intensity for the particular application.

** Managed by UT-Battelle, LLC, for the US Department of Energy under contract DE-AC05-00OR22725.

12.2 Beam Extraction and Beam Quality Definitions

12.2.1 Beam Extraction

A number of sophisticated codes have been developed for simulating the actions of electric and magnetic fields on charged-particle beams during extraction of space-charge-dominated ion beams from plasma ion sources [35–40]. These codes have enabled the design of a variety of beam transport components, as well as the simulation of ion extraction from solid and plasma emitters. Such codes simulate the actions of the fields on charged ions moving through or accelerated by such fields. Poisson's equation

$$\nabla^2\phi = -\rho/\varepsilon_0 \tag{12.1}$$

is solved at each point within the configuration using space-charge densities computed from the collective influence on the particle trajectories within the beam. In (12.1), ϕ is the electric potential, ρ is the charge density and ε_0 is the permittivity of free space.

The Positive-Ion Current

Sputter-type sources can be categorized according to the means of producing the positive-ion beam used to sputter the sample. Several sources utilize direct surface ionization of cesium vapor as it comes in contact with a hot, high-work-function surface to form positive ions, which are then accelerated against a negatively biased probe (cathode) containing the material of interest.

Extraction of beams at an extraction voltage $\Delta\phi_{ex}$ under conditions where ρ in (12.1) limits the ion beam current I (the value of the current that can be extracted) obeys the Child–Langmuir relation, given by $I = P\,\Delta\phi_{ex}^{3/2}$, where P is the perveance of the particular electrode system. For a parallel-plate electrode system, the perveance is

$$P_{pp} = \{4\varepsilon_0/9\}\,[2qe/M]^{1/2}\,\pi a^2/d^2 \tag{12.2}$$

where a is the radius of the emission aperture (circular apertures), d is the electrode spacing and M is the mass of the extracted ion species. In general, P varies from system to system because of differences in geometry and electrode design.

Optimum Perveance

The perveance for a given electrode system can be expressed in terms of the perveance P_{pp} for the parallel-plate electrode system, according to $P_{opt} \cong fP_{pp}(d_{opt})$, where f is a factor that varies from electrode system to electrode system [41].

The Negative-Ion Current

According to [41], when ions are extracted from a plasma, the plasma boundary has an optimum concave radius of curvature that minimizes the angular divergence from the source and thereby minimizes the emittances of extracted beams. Thus, the extracted current has an optimum value, given by

$$I_{opt} = P_{opt}(d_{opt})\,\Delta\phi_{ex}^{3/2} = fP_{pp}(d_{opt})\,\Delta\phi_{ex}^{3/2} \tag{12.3}$$

The value of the perveance at the minimum half-angular divergence ($\omega \cong 0$) is referred to the optimum perveance P_{opt}. The factor f is approximately 0.6 for extraction of space-charge-limited currents from a parallel-plate electrode system, and $f \cong 0.49$ for extraction from a two-electrode, spherical-geometry system [41].

12.2.2 Liouville's Theorem

Liouville's theorem states that the motion of a group of particles under the action of conservative fields is such that the local number density in the six-dimensional phase space volume (hypervolume) $xyzp_xp_yp_z$ everywhere remains constant. The theorem applies to an ion beam subjected to conservative fields. The quality of an ion beam is usually expressed in terms of the emittance ε and brightness B. Both are related to Liouville's theorem.

12.2.3 Emittance

For DC beam transport, the components of phase space transverse to the direction of beam motion are usually the most important. If the motions of the particles in the orthogonal planes (x, p_x), (y, p_y) and (z, p_z) are uncoupled, the phase spaces associated with each of these planes will be separately conserved. These conserved area in the respective direction of motion is referred to as the emittance ε of the ion beam in the given direction. The conserved components of transverse phase space are taken to be elliptical in shape, the areas of which are given by $A_x = \pi\{xp_x/\pi\}$ and $A_y = \pi\{yp_y/\pi\}$. For the case where the component of momentum along the z-direction of the beam is approximately constant,

$$\begin{aligned} A_x &= \pi\{xp_z \tan\theta_{xz}/\pi\} = \pi\{xM_2 \tan\theta_{xz}/\pi\}\beta\gamma c \\ A_y &= \pi\{yp_z \tan\theta_{yz}/\pi\} = \pi\{yM_2 \tan\theta_{yz}/\pi\}\beta\gamma c \end{aligned} \tag{12.4}$$

where $\beta = v/c$ and $\gamma = 1/[1 - \{v/c\}^2]^{1/2}$. M_2 is the mass of the particle, of speed v; c is the speed of light; and θ_{xz}, θ_{yz} are the angles that the projection of the particle's velocity in the xz and yz-planes make with the z-direction (direction of motion). In the small-angle approximation, $\tan\theta_{xz} = \theta_{xz} = dx/dz = x'$ and $\tan\theta_{yz} = \theta_{yz} = dy/dz = y'$, so that

$A_x = \pi\{xx'M_2/\pi\}\beta\gamma c$ and $A_y = \pi\{yy'M_2/\pi\}\beta\gamma c$ (relativistic case). For the nonrelativistic case, $A_x = \pi\{xx'/\pi\}[2EM]^{1/2}$ and $A_y = \pi\{yy'/\pi\}[2EM]^{1/2}$, where E is the energy of the ion beam. The emittance ε of the ion beam is proportional to the transverse phase space and thus is a conserved quantity. The following definitions related to the energy E and velocity v have been adopted historically for the normalized emittances ε_{nx} and ε_{ny}:

$$\varepsilon_{nx} \approx \pi \int\int [dx\, dx'/\pi]\ ;\ \ \varepsilon_{ny} \approx \pi \int\int [dy\, dy'/\pi] \tag{12.5}$$

or

$$\varepsilon_{nx} \approx \pi \int\int [dx\, dx'/\pi]\sqrt{E};\ \ \varepsilon_{ny} \approx \pi \int\int [dy\, dy'/\pi]\sqrt{E} \tag{12.6}$$

where the integrations are performed over the emittance contour that contains a specified fraction of the beam (e.g. 10%, 20%, ... 90%, etc.) Equation (12.6) has been historically adopted as defining the normalized emittance in the electrostatic-accelerator community.

12.2.4 Brightness

Another figure of merit, often used for evaluating the properties of ion beams, is the brightness B. Brightness is defined in terms of the ion current dI per unit area dS and per solid angle $d\Omega$, or $B = d^2I/dS\, d\Omega$. The normalized brightness B_n can be expressed as $B_n = 2d^2I/\varepsilon_{nx}\varepsilon_{ny}$ [42].

The normalized root-mean-square (RMS) emittance $\varepsilon_{n,RMS}$ and the normalized physical emittance ε_n are usually defined according to the following formulas:

$$\begin{aligned}\varepsilon_{n,RMS}(x,x') &= \pi[(\langle x^2\rangle\langle x'^2\rangle - \langle xx'\rangle^2)/\pi^2]^{1/2}\beta\gamma \\ \varepsilon_{n,RMS}(y,y') &= \pi[(\langle y^2\rangle\langle y'^2\rangle - \langle yy'\rangle^2)/\pi^2]^{1/2}\beta\gamma\end{aligned} \tag{12.7}$$

where the relationship between $\varepsilon_{n,RMS}$ and ε_n (90% contour value) is often defined as

$$\varepsilon_n(x,x') = 4\varepsilon_{n,RMS}(x,x');\ \ \varepsilon_n(y,y') = 4\varepsilon_{n,RMS}(y,y') \tag{12.8}$$

In this context, the normalized RMS brightness $B_{n,RMS}$ is defined by $B_{n,RMS} = 2d^2I/\{\varepsilon_{nx,RMS}(x,x')\varepsilon_{ny,RMS}(y,y')\}$, where dI is the ion beam current within a specified emittance contour.

12.3 The Negative-Ion State

12.3.1 The Electron Affinity

The processes involved in the attachment of electrons to neutral atoms or molecules to form negative ions are exothermic, in contrast to the endothermic

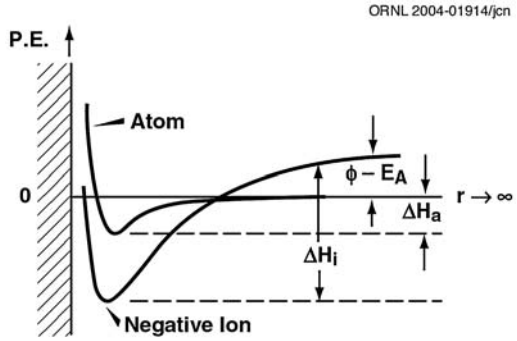

Fig. 12.1. Potential-energy curve for an atom and negative ion as a function of distance from a hot metal surface. ϕ is the work function of the metal; ΔH_a and ΔH_i are the respective enthalpies of adsorption for the atom and ion; and E_A is the electron affinity of the atom

processes required for positive-ion formation. The parameter that characterizes the negative-ion state is the binding energy of the additionally attached electron, or the electron affinity, E_A. The electron affinity of a negative ion is a measure of the stability and ease of ion formation, as well as ease of detachment, and therefore is defined as the difference between the energy of the neutral ground state E_0 and the energy of the negative ion E_-, or $E_A = E_0 - E_-$. E_A must be positive to form a stably bound negative-ion state.

Consider the potential energy of an atom with electron affinity E_A as a function of the distance from the surface of a metal of work function ϕ, as illustrated in Fig. 12.1. The energy required for removing the ion from the surface is ΔH_i, and the condition for residing on the surface as an ion is $\Delta H_i - (\phi - E_A) > \Delta H_a$, where ΔH_a is the enthalpy of adsorption. An ion supplied with an energy ΔH_i may be transferred to the continuum in either ionic or atomic form in cases where the potential-energy curves cross. At a distance far from the influence of the metal on the affinity level of the atom, the atomic and ionic potential curves will be separated by an amount $(\phi - E_A)$. The probability of arrival at a position far from the metal in a given state depends on the magnitude of $(\phi - E_A)$.

12.3.2 Electron Affinities of the Elements and of Molecules

Approximately 78% of the naturally occurring elements have positive electron affinities. Figure 12.2 displays first ionization potentials and electron affinities of the elements [3–20]. The electron affinities have values ranging from $E_A \leq 0$, to $E_A = 3.613\,\text{eV}$ for Cl. Notable examples of elements with negative electron affinities are Be [4,9] and Mg [4] of the group IIA elements, N of the group VA elements [4], Mn of the group VIIB elements [4], and all members

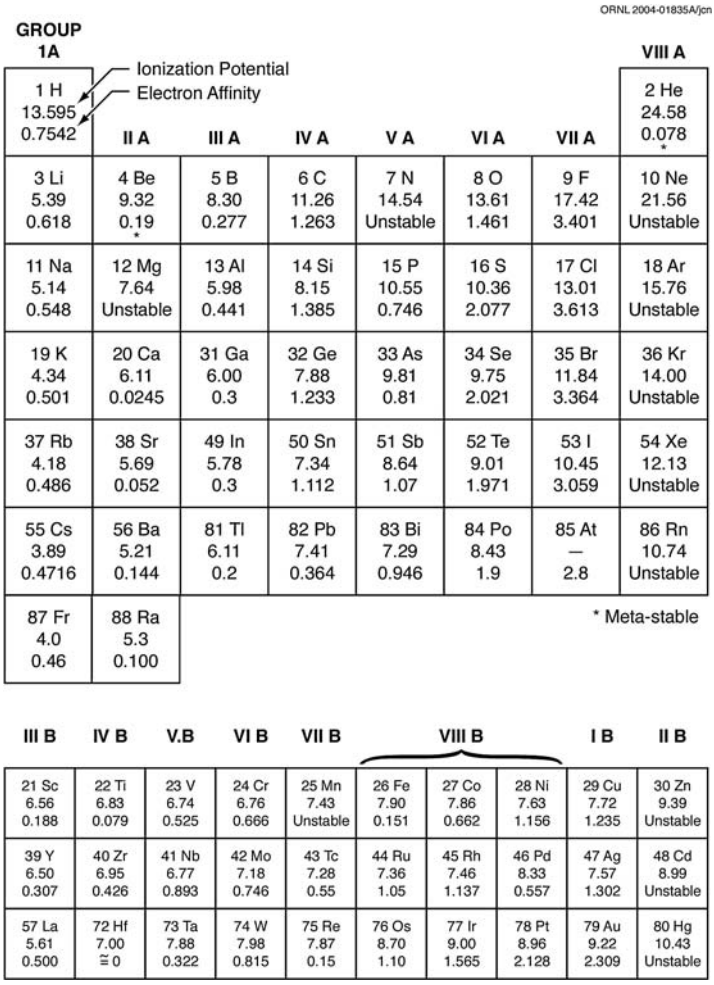

Fig. 12.2. Electron affinities and ionization potentials of the elements in eV

of the group IIB elements (Zn, Cd and Hg) [4] and VIIIA elements (He, Ne, Ar, Kr, Xe and Rn) [4], while Hf is estimated to have an electron affinity $E_A \cong 0$ [4].

The group IIA elements span the complete spectrum of possible electron affinities. Be has a negative ground-state electron affinity, but is bound metastably in the $1s^2 2s 2p^2 (^4P)$ state; the ion is metastable against spin–spin interactions, has a lifetime of a few μs and thus lives long enough for practical use [4, 9]. Mg, on the other hand, forms neither a bound ground state nor a metastably bound state and thus cannot be produced as an atomic negative ion [4].

In addition to negative atomic species, many molecular negative ions have been observed. In many cases, molecular negative ions containing the atom of interest have much higher electron affinities than has the atom itself and, therefore, can be formed with higher probability than the atomic species can be. In some cases, molecular ions offer the only alternative for producing beams containing elements that do not form stably bound negative-ion states. For tandem electrostatic-accelerator applications, the unwanted species can be easily rejected by collision dissociation in the positive-ion formation process (stripping) followed by magnetic (M/q) analysis for selection of the atomic species of interest. Electron affinities of a selected number of diatomic, triatomic and polyatomic molecular species are tabulated in Table 12.1 [21–33].

Table 12.1. Electron affinities (E_A) in eV of selected diatomic, triatomic and polyatomic molecules

Molecule	E_A	Molecule	E_A	Molecule	E_A
Al_2	1.10	Al_3	1.40	SF_4	2.35
BO	3.12	BO_2	3.57	SF_6	1.05
BeH	0.7	CoH_2	1.45	TeF_6	3.34
C_2	3.269	Cs_3	0.864	UF_5	4.4
CH	1.238	K_3	0.956	UF_6	5.1
CN	3.821	N_3	2.70	WF_5	1.25
CaH	0.93	NO_2	2.273	WF_6	3.36
Co_2	1.110	Na_3	1.019		
CrO	1.222	PH_2	1.271		
Fe_2	0.902				
FeH	0.934				
MgH	1.05				
MnH	0.869				
NS	1.194				
OH	1.827				
PH	1.028				
PO	1.092				
Re_2	1.571				
ZnH	0.95				

12.3.3 Metastable-Negative-Ion Formation

There is an important class of negative ions that can be formed in excited states of the parent atom and live long enough to be useful. In order to induce electron attachment and thus form such metastable states, it is necessary to form the particular excited electronic state of the neutral atom to which

an electron can be attached. The charge transfer process (discussed later in this chapter) is particularly well suited for metastable-ion formation. The subsequently formed negative ion may live for extended periods of time if the excited compound state is forbidden to decay. Classic examples of metastable negative ions that can be formed only through attachment to excited states of the parent atoms are He^- [4–8] and Be^- [4, 9], both forming with high probability in the ^4P state through sequential charge exchange with a low-ionization-potential charge exchange vapor.

12.4 Negative-Ion Formation in a Plasma Environment

12.4.1 Radiative Electron Capture and Dielectronic Attachment

The simplest way to form negative ions is by direct capture of a free electron by a neutral atom. However for attachment to take place, the difference between the kinetic energy of the electron and electron affinity of the atom must be conserved through photon emission or momentum transfer to the motion of the atom.

Another attachment mechanism is possible, involving radiative stabilization. Attachment is possible if the incident electron has an energy such that the energy of the atom plus electron is within the level width of a doubly excited state of the atom. Thus, it is possible to capture the electron by reverting to the ground state by radiative emission; the atom may revert back to the neutral by ejecting the electron back into the continuum. Radiative electron capture and dielectronic attachment are low-probability processes and, therefore, not important in high-intensity negative-ion sources.

12.4.2 Polar Dissociation Attachment

Polar dissociation attachment may occur as a result of interactions with molecular neutrals in which sufficient energy is imparted to the molecule to excite it to an unstable state that dissociates spontaneously into positive and negative ions. Polar photodissociative attachment is a process whereby a molecule XY absorbs a photon of sufficient energy to cause spontaneous fragmentation according to the reaction

$$XY + h\nu \rightarrow X^- + Y^+ \tag{12.9}$$

Negative-ion formation may also occur by this mechanism whenever an electron of sufficient energy for molecular excitation to an unstable state interacts with a molecule XY as follows:

$$e + XY \rightarrow X^+ + Y^- + e \tag{12.10}$$

We note that the electron is not itself captured, but only serves as the means by which the molecular excitation occurs.

12.4.3 Dissociation Attachment

Electrons may be stably attached to atoms during interactions with molecular neutrals according to the following process:

$$e + XY \rightarrow X^- + Y \tag{12.11}$$

The process may be viewed as a three-body process where the excess energy released during the reaction can be absorbed by transfer to the relative motion of the atomic nuclei or fragments, and thus the state can be readily stabilized.

On the other, hand attachment to a molecule can occur for molecules with positive electron affinities without dissociation, thereby forming a molecule XY^-. Vibrational states of the molecule will be stable for frequencies $\nu < \nu'$; those with vibrational frequencies $\nu > \nu'$ will be unstable toward autodetachment. Again, this process is possible because electronic excitations take place on a timescale short with respect to the motion of nuclei (Franck–Condon principle).

12.4.4 Ternary Collisions Between Electrons and Molecules

Three-body or ternary collisions are the most efficient in producing negative ions in a dense gas or plasma at low electron energies. These occur as follows:

$$\begin{aligned} e + X + Y &\rightarrow X^- + Y \\ X + 2e &\rightarrow X^- + e \end{aligned} \tag{12.12}$$

The first process is of much greater practical importance, because the second occurs only in systems with high electron densities.

12.4.5 Volume-Production Heavy-Negative-Ion Sources

While all of the previously discussed radiative and collisional electron capture processes may take place in certain types of negative-ion sources at some rate, radiative and dielectronic capture are known to be low-probability processes and, therefore, are not practical mechanisms for negative-ion formation. In most sources that utilize charged particles for production (electrons or ions) photopolar dissociation processes are infrequent because of the low-photon-flux environment. In plasma-type negative-ion sources, electron impact polar dissociation, dissociative attachment and three-body collisional transfer processes dominate. Sources that employ electron impact attachment methods to form negative ions directly in a plasma medium are often called direct-extraction sources. Almost any positive plasma discharge source can be used to generate negative-ion beams by simply operating the source in reverse polarity. It is now well understood that the addition of Cs or other group IA elements into plasma discharges enhances negative-ion formation. In general, plasma sources have very good beam qualities, particularly those that rely on dissociative electron attachment.

Duoplasmatron-Type Heavy Negative-Ion Sources

Moak et al. [43] first discovered that useful intensities of negative ions could be directly extracted from a duoplasmatron when operated in reverse polarity. Later it was discovered that negative ions were more abundant in the periphery of the plasma and that the yields could be enhanced by offsetting the extraction electrode with respect to the center of the plasma [44]. Other negative direct-extraction versions of the duoplasmatron source have been described in the literature, including the duodecatron [45] and triplasmatron [46]. The duodecatron has produced >100 μA of H^- and >10 μA of O^-, F^- and Cl^-, while the triplasmatron has produced >50 μA of O^-.

Diode Heavy-Negative-Ion Sources

A diode source [47] has been used to generate several negative-ion species, including 600 μA H^-, 20 μA BO^-, 0.5 μA C^-, 10 μA CN^-, 4 μA O^-, 50 μA F^-, 4 μA P^- and 4 μA S^-.

Penning Discharge Heavy-Negative-Ion Sources

A radial-geometry cold-cathode Penning discharge source [48] has been utilized to generate a variety of DC negative-ion beams, including 60 μA H^-, 1.2 μA Li^-, 0.2 μA BeH^-, 1.0 μA MgH^-, 100 μA F^-, 10 μA B^-, 50 μA S^- and 50 μA Cl^-. The materials to be ionized are fed into the plasma discharge as gases, vaporized from an oven or sublimed from a solid rod of the material. This source type has also been used to generate 2.7 μA C^-, 6.5 μA Cu^- and 4 μA Ni^- by sputtering solid rods made of the material of interest submerged in the plasma discharge [49].

12.5 Negative-Ion Formation Through Charge Exchange

During collisions between an ion neutral atom or molecule and another ion, neutral atom or molecule, an electron can be transferred from one of the colliding partners to the other with high probability, depending on the collision energy, ionization potentials and electron affinities of the colliding partners. A single charge transfer process is often referred to as "charge exchange" or "electron capture". The charge transfer process can be categorized according to the energy defect ΔE involved in the transfer, as defined by the following interaction of the projectile X and target Y:

$$X^+ + Y \rightarrow X + Y^+ + \Delta E_1 \tag{12.13}$$

where ΔE_1 is just equal to the difference in ionization energies E_i of the colliding partners. For negative-ion formation, the energetic neutral atom X must undergo a second collision, as represented by the following reaction:

$$X + Y \rightarrow X^- + Y^+ + \Delta E_2 \tag{12.14}$$

where ΔE_2 is the difference between the electron affinity $E_A(X)$ of X and the ionization energy $E_i(Y)$ of Y.

In general, the charge-transfer collision takes place at relatively large impact parameters, in which the projectile scattering angle is small and the product ion is scattered nearly perpendicular to the impact momentum vector. From the standpoint of beam quality degradation, low-momentum-transfer processes are clearly desirable. Such transfer processes can be cast into two distinct categories: (1) symmetrical (resonance) processes, and (2) asymmetrical (nonresonance) processes. In the first category, the projectile and target are the same species, while in the latter, practically more important category, the projectile and target are different.

12.5.1 Symmetrical (Resonance) Charge Exchange

In the symmetrical charge transfer process, in which the projectile and target are identical, the energy defect is equal to the difference between the ionization energies and is thus zero. Hence the cross sections can be very large. Negative-ion formation requires the following sequential projectile–target reactions:

$$\begin{aligned} &X^+ + X \rightarrow X + X^+ + \Delta E \quad (\Delta E = 0) \\ &X + X \rightarrow X^- + X^+ + \Delta E \quad (\Delta E = E_A(X) - E_i(X)) \end{aligned} \tag{12.15}$$

As noted, the energy defect for the second reaction is equal to the difference between the electron affinity of the first projectile atom E_A and the ionization energy E_i of the stationary target atom. Thus, a symmetrical process may not necessarily be commensurate with efficient negative-ion formation because of the possibility of a high ionization energy E_i for the donor species. However, consideration may be given to a two-step process in which the first process is symmetrical, and for which the cross section is large for neutral-energetic-atom formation, followed by an asymmetrical nonresonance process in which the energy defect is much smaller. Obviously, the energy defect can be minimized by selection of a charge transfer medium which has a low first ionization energy. Cesium has the lowest ionization energy of the naturally occurring group IA elements and is easy to volatilize. However, because of its high atomic number and mass, scattering is exacerbated relative to lower-mass members of this group such as Li. Li, however, is more difficult to use because of the relatively high temperatures required to volatilize the material.

12.5.2 Asymmetrical (Nonresonant) Charge Exchange

The formation of negative-ion beams by a two-step symmetrical/asymmetrical process would be impractical for general use, since it would involve the use of

two different charge exchange media, the first identical to that of the projectile and the second chosen because of the ease of transferring electrons to the energetic projectile X. The most general application of the charge exchange formation technique is for interactions between unlike ions. These processes occur with high probability between projectiles interacting with exchange vapors that possess a low energy defect. The probability for charge transfer from the electron donor (exchange vapor) to the projectile ion is sensitively dependent on the speed of the projectile.

The atomic charge transfer process occurs between unlike ions and differs from the symmetric resonance process in that it involves an electronic transition that requires a change in the internal energy of the system, or an energy defect ΔE. The energy defects ΔE_1 and ΔE_2 involved in the asymmetrical charge exchange formation of negative ions can be symbolically expressed through the following reactions:

$$\begin{aligned} X^+ + Y &\rightarrow X + Y^+ + \Delta E_1 \\ X + Y &\rightarrow X^- + Y^+ + \Delta E_2 \end{aligned} \tag{12.16}$$

ΔE_1 can be equated to the difference between the ionization energies E_i of the interacting atoms or molecules as

$$\Delta E_1 = E'(X^+) - E(X) + E(Y) - E(Y^+) = E_i(X) - E_i(Y) \tag{12.17}$$

while the energy defect E_2 is given by

$$\Delta E^2 = E(X) - E(X^-) + E(Y) - E(Y^+) = E_A(X) - E_i(Y) \tag{12.18}$$

Two-electron capture during a single collision is much less likely owing to the very high energy defect.

12.5.3 The Massey Adiabaticity Criterion

The adiabatic criterion proposed by Massey is of practical importance in asymmetrical charge transfer collisions [50]. At low projectile impact energies where the relative motion of the atoms is slow enough that the electronic motion can adiabatically adjust to small changes in the internuclear distance, the electron transfer process becomes unlikely. However, if the impact energy falls outside this "adiabatic region" and the electronic transition time is comparable to the collision time, the probability for electron transfer can be very high. The time of collision is taken as a/v, where v is the impact speed and a, the "adiabatic parameter", is of the same order as the atomic dimensions within which the charge transfer transition becomes likely. The characteristic time for the electronic transition is given by $h/\Delta E$, where ΔE is the energy defect. Thus, the condition $v \ll (a|\Delta E|)/h$ characterizes the adiabatic speed region, and $v \cong (a|\Delta E|)/h$ characterizes the speed region for which the maximum in the charge transfer process occurs.

The projectile energy E_{1MAX} for which the cross section reaches its maximum for a given reaction is given by

$$E_{1MAX} = F\{M_1/2\}(a\,\Delta E/h)^2 \tag{12.19}$$

where F is a constant, adjusted to bring the equation into better agreement with experimental measurement. Since two energy defects ΔE are involved in the negative-ion formation process involving a single exchange medium, the Massey adiabatic-maximum rule represented by (12.19) cannot simultaneously meet both optimum values. Consequently, the optimization process is ultimately a compromise between the two optimum values. However, in testing (12.19), it was found that best agreement with experiment came whenever the last reaction was taken as the dominant process. In practical units, (12.19) becomes

$$E_{1MAX}[\text{keV}] = 8.31 \times 10^{-3} M_1[\text{amu}][a(\text{Å})\Delta E_2(\text{eV})]^2 \tag{12.20}$$

The criterion has been applied by Hasted to many charge transfer cross sections for reactions to estimate projectile energies that maximize negative-ion generation rates (maximum cross sections) [51]. Equation (12.20) has been applied by the present author to equilibrium fraction versus projectile speed data for $^{23}Na^+$, $^{27}Al^+$, $^{31}P^+$, $^{69}Ga^+$, $^{74}Ge^+$, $^{75}As^+$, $^{116}Sn^+$ and $^{208}Pb^+$ passing through ^{133}Cs vapor under the assumption that the criterion holds as an equality at the respective energy. The results of the latter calculations are given in Table 12.2. As noted, reasonable agreement is found for most of the species. The "adiabatic-maximum rule" is taken as a practical method for approximating optimum projectile energies for producing negative ions through charge exchange.

Table 12.2. Measured energy maxima and values calculated using (12.20) for charge exchange generation of selected negative-ion beams in Cs vapor

Projectile	a	ΔE_2(eV)	E_{MAX}(keV) (measured)	E_{MAX}(keV) (calculated)
Na^+	2.29	3.342	∼14.5	11.2
Al^+	2.05	3.449	∼20.2	11.2
P^+	1.97	3.144	∼5	9.9
Ga^+	2.04	3.59	∼41.5	30.8
Ge^+	2.02	2.657	∼15.5	17.7
As^+	2.03	3.08	∼15.5	24.4
Sn^+	2.15	2.778	∼24	34.4
Pb^+	2.21	3.526	∼35.5	105

12.5.4 Charge Exchange Cell Design

Since operational lifetime is of primary concern, special attention is given to cell design. Cell designs have increased in efficiency and lifetime in recent years, primarily because of the advent of sophisticated thermal simulation codes for accurately modeling thermal gradients in these devices. By accurately modeling thermal gradients in relation to the physical design of the cell and the materials of construction, the operational lifetimes of charge exchange cells can be very long. A cross-sectional view of a long-lifetime Li, Na, Mg or Ca cell, designed for use in producing radioactive ion beams (RIBs), is displayed in Fig. 12.3 [52]. By maintaining temperature gradients along the beam entrance and exit nozzles, the cell design ensures that the donor vapor condenses, liquefies and drains back into the reservoir along the slope of each nozzle. As noted, the cell is equipped with pneumatically actuatable Faraday cups, located at the entrance and exit of the cell to aid in characterization of the cell (measuring transmission and charge exchange efficiencies of species of interest). The cell uses heaters clamped against the body of the stainless steel cell for heating the elemental charge exchange material to the temperature that optimizes the vapor density in the path of the beam. A temperature of $\sim$450°C produces a near-optimum target thickness ($\sim 1 \times 10^{15}\,\mathrm{cm}^{-3}$).

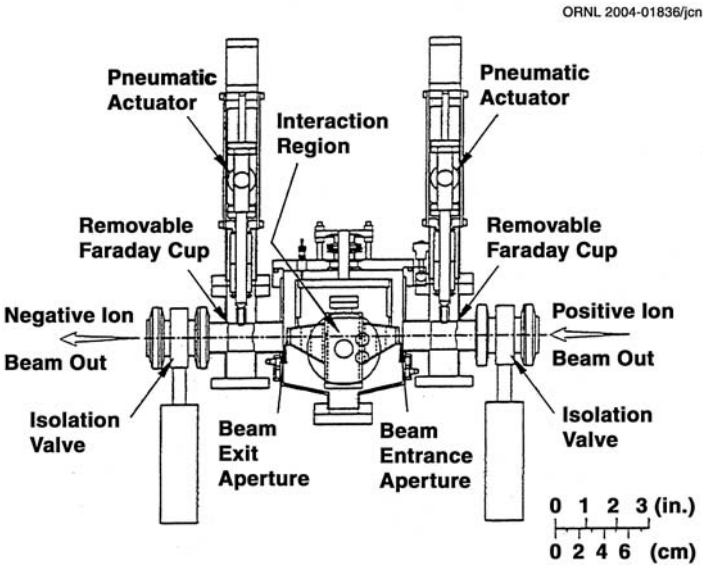

Fig. 12.3. A cross-sectional view of a long-lifetime Li, Na, Mg or Ca cell, designed for use in producing radioactive ion beams (RIBs) [52]

12.5.5 Charge Exchange Sources

The positive-ion source may be a simple gas source such as a duoplasmatron or RF source or a more universal source capable of producing positive-ion beams of volatile compounds. A schematic illustration of a duoplasmatron close-coupled to a Ca charge exchange cell is illustrated in Fig. 12.4.

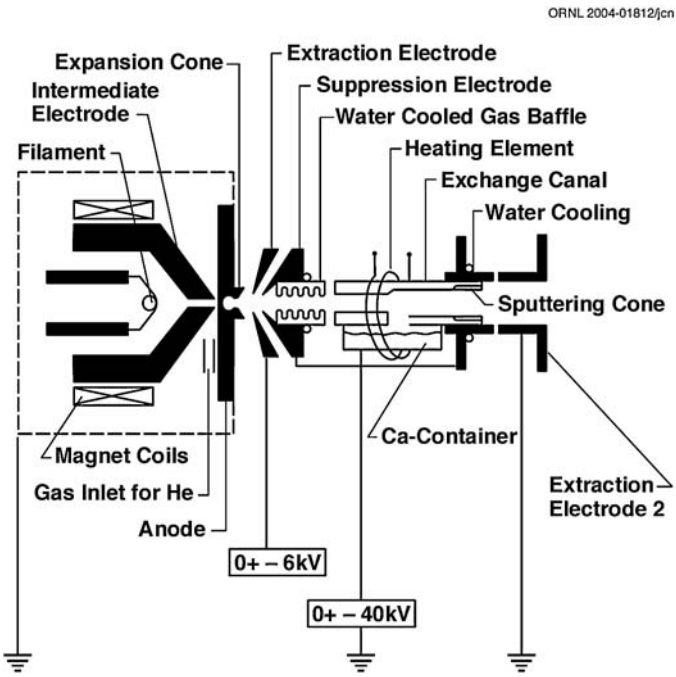

Fig. 12.4. Schematic representation of a close-coupled duoplasmatron positive-ion source and Ca vapor cell charge exchange system

12.5.6 Beam Quality Degradation Effects

In practice, consideration must be given to ease of loading, handling and ease of volatility of the donor material when designing k charge-exchange cell. In this regard, Rb or Cs is well suited for use. However, the charge exchange process can induce energy spreads of several hundred eV into beams. By its collisional nature, the charge exchange process degrades the quality of beams. For example, the mass of the primary beam in relation to the mass of the donor material is important. Ideally, a light donor material is best suited for use, since the maximum energy transfer E_{2max} is given by

$$E_{2max} = 4M_1M_2E_1/(M_1 + M_2)^2 \tag{12.21}$$

M_1 represents the mass of the primary beam of energy E_1, and M_2 the mass of the donor material. Maximum energy transfer occurs whenever the masses of the primary beam and donor material are the same. The energy and angular spread resulting from passage of C^+, Na^+, Al^+, P^+, Ga^+, Ge^+, As^+, Sn^+ and Pb^+ projectiles at the optimum energies for charge conversion in $1.1 \times 10^{15}\,cm^{-3}$ Li, Na, K, Rb and Cs charge exchange vapors are displayed in Tables 12.3 and 12.4, respectively.

Table 12.3. Energy spread (in keV) induced in various projectiles during charge exchange conversion from positive to negative ions in Li, Na, K, Rb and Cs vapor. Target density $1.1 \times 10^{15}\,cm^{-3}$ and length 10 cm

Projectile	Energy (keV)	Li	Na	Mg	K	Ca	Rb	Cs
C^+	20	0.015	0.093	0.095	0.18	0.18	0.45	0.68
Na^+	14.5	0.011	0.069	0.070	0.13	0.13	0.30	0.37
Al^+	20.2	0.012	0.070	0.075	0.14	0.14	0.33	0.43
P^+	5	0.014	0.068	0.068	0.10	0.11	0.23	0.28
Ga^+	41.5	0.018	0.094	0.090	0.16	0.16	0.34	0.55
Ge^+	15.5	0.029	0.10	0.12	0.19	0.18	0.34	0.45
As^+	15.5	0.027	0.11	0.12	0.19	0.18	0.33	0.43
Sn^+	24	0.044	0.17	0.18	0.29	0.27	0.42	0.49
Pb^+	35.5	0.090	0.34	0.38	0.47	0.51	0.76	0.72

Table 12.4. Angular spread (in mrad) induced in various projectiles during charge exchange conversion from positive to negative ions in Li, Na, K, Rb and Cs vapor. Target density $1.1 \times 10^{15}\,cm^{-3}$ and length 10 cm

Projectile	Energy (keV)	Li	Na	Mg	K	Ca	Rb	Cs
C^+	20	5.0	19	19	27	27	59	78
Na^+	14.5	9.8	45	43	64	63	100	120
Al^+	20.2	8.5	40	35	55	54	94	110
P^+	5	39	130	130	190	200	320	410
Ga^+	41.5	8.6	28	28	45	41	73	86
Ge^+	15.5	22	71	72	110	110	160	220
As^+	15.5	22	77	73	110	110	170	210
Sn^+	24	19	58	57	85	85	150	180
Pb^+	35.5	16	50	53	76	82	130	170

12.5.7 Negative-Ion Equilibrium Fractions

The differential fraction of negative ions dF_i produced during passage through a vaporous target of thickness $d\pi$ can be expressed in terms of a set of first-order linear differential equations given by

$$dF/d\pi = \sum F_j \sigma_{ji} - \sum F_i \sigma_{ij} \tag{12.22}$$

Solution of the set of coupled equations requires the knowledge of $n(n-1)$ cross sections for a system involving n states.

Negative-ion conversion from an initially positive-ion beam interacting with a low-ionization-potential vapor can take place with high probability. The mechanism is therefore a very practical method for the production of negative-ion beams and has been utilized for this purpose for several years. As first shown experimentally by Donnally and Thoeming [53], the electron transfer process involves the transfer of a single electron in sequential collisions between the projectile and charge exchange atoms/molecules. As noted in (12.19) and (12.20), the production efficiencies depend primarily on the ion energy, the electron affinity of the element under consideration and the first ionization potential of the donor material. Several donor materials, including Li, Na, Mg, Ca, Rb and Cs, have been utilized as charge exchange media. The choice of medium affects the probability of ion formation as well as beam quality. Experimental schemes for measuring equilibrium fractions of negative ions have been described by several groups [54–56].

Equilibrium fractions for H in several group IA and group IIA vapors and for D in various group IA vapors have been measured [57]. The corresponding equilibrium fraction data for H are shown in Fig. 12.5. Many other investigations have been made of probabilities and energy dependences of charge transfer negative-ion formation, including H in Na [58] and Cs [59] vapors, and He in Li, Na and Mg [60], K [61], Rb [62], and Cs [63] vapors.

Extensive and systematic investigations of the charge exchange process for the production of many ion species have been carried out using Mg [55], Na [56] and Cs [64] vapors by researchers at the University of Aarhus. These investigations show efficiencies ranging from $\sim 0.5\%$ to $>90\%$. Mg is a more effective electron donor for high-electron-affinity elements, while Na is more effective for low-electron-affinity elements. Further evidence of the efficiency and universal character of the charge transfer process is found for group IA, IIIA, IVA and VA projectiles in cesium vapor in [64]. The corresponding equilibrium fraction dependences for these groups of elements on the projectile velocity in Cs vapor are displayed in Fig. 12.6. As noted, the maximum efficiency appears to occur at a rather well-defined velocity for each group of elements and does not vary much from group to group. Such information is very useful in selecting the most appropriate particle energy for optimizing the charge exchange efficiency when Cs is used as the donor material.

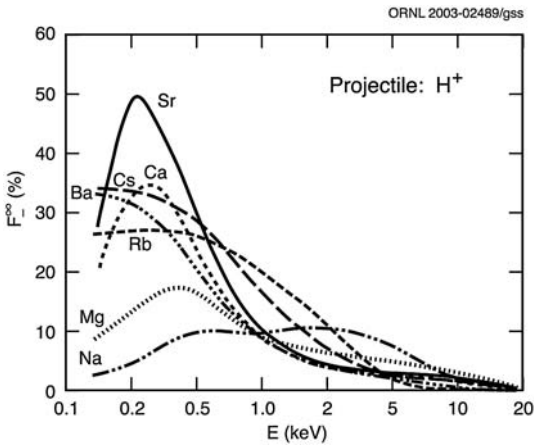

Fig. 12.5. Negative-ion equilibrium yields F_{-}^{∞} versus projectile energy E for H^+ in several group IA (Na, Rb and Cs) and group IIA (Mg, Ca and Ba) vapors [57]

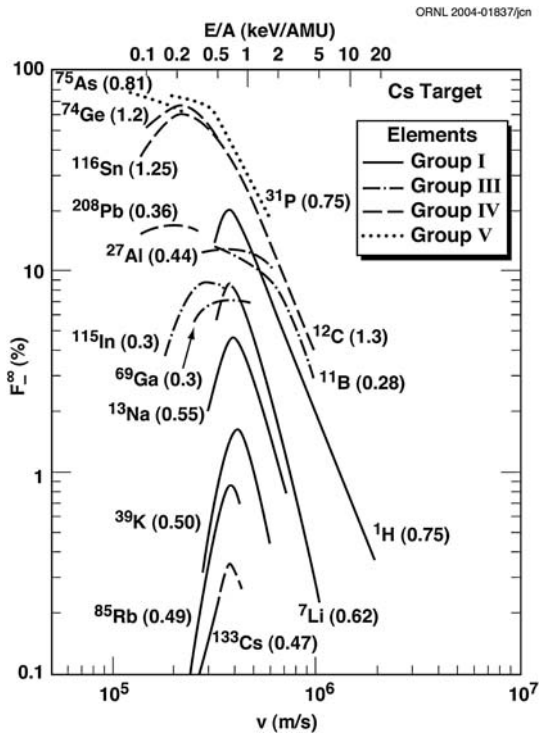

Fig. 12.6. Negative-ion equilibrium fractions F_{-}^{∞} versus projectile speed v for a few group IA, IIIA, IVA and VA elements [64]

12.6 Thermodynamic-Equilibrium Surface Ionization

Atoms or molecules impinging on a hot metal surface may be emitted as positive or negative ions in subsequent evaporation processes. The process of direct surface ionization is statistical in nature, and therefore thermodynamic arguments can be applied in deriving equations for the degree of positive- or negative-ion formation under equilibrium conditions. The subject has been reviewed in [65]. Experimental methods for negative-ion production by surface ionization have been reviewed by Kawano et al. [66–68].

12.6.1 Theory of Negative Surface Ionization

As discussed previously, the energy required for removing an ion from the surface is $\Delta H_i - (\phi - E_A) \geq \Delta H_a$. An ion supplied with energy ΔH_i may be transferred to the continuum in either ionic or atomic form where the respective potential-energy curves cross. The probability for arrival at a position far from the metal in a given state depends on the magnitude of $(\phi - E_A)$.

The probability P_i for negative-ion formation of a neutral particle of electron affinity E_A, evaporated from a hot surface with a low work function ϕ at temperature T, is given by the Langmuir–Saha relation

$$P_i = \frac{\omega_-}{\omega_0}\left(\frac{1-r_-}{1-r_0}\right)\exp\left(\frac{E_A-\phi}{kT}\right) \times\left[1+\frac{\omega_-}{\omega_0}\left(\frac{1-r_-}{1-r_0}\right)\exp\left(\frac{E_A-\phi}{kT}\right)\right]^{-1} \tag{12.23}$$

where r_- and r_0 are the reflection coefficients of the particle at the surface and ω_- and ω_0 are statistical weights for the negative ion and neutral atom, respectively. ω_- and ω_0 are related to the total spin of the respective species and are given by $\omega = 2\sum_i s_i + 1$, where s_i is the spin of the electron. Equation (12.23) describes an idealized situation in which there is perfect isotropy and no contamination of the ionizer surface. Moreover, the work function varies with crystalline orientation in cases where the metal is polycrystalline or the surface has uniformly or nonuniformly distributed surface contaminants. All of these effects can be taken into account by approximately summing over admixtures of existing work functions and statistical weighting factors in the respective expressions. From the relationship, it is evident that negative-ion yields could be enhanced by lowering the work function ϕ, or by increasing the surface temperature T for elements where $E_A \leq \phi$. In practice, ϕ varies with the crystalline orientation, and adsorption of highly electronegative atoms or molecules such as oxygen or the halogens raises the work function. Such contaminants can raise the work function and destabilize the formation process, and thus are the bases of the poisoning effects that will be discussed later. The computed efficiency (12.23) for negatively ionizing selected atoms and molecules striking a clean, hot LaB_6 surface is shown in Fig. 12.7.

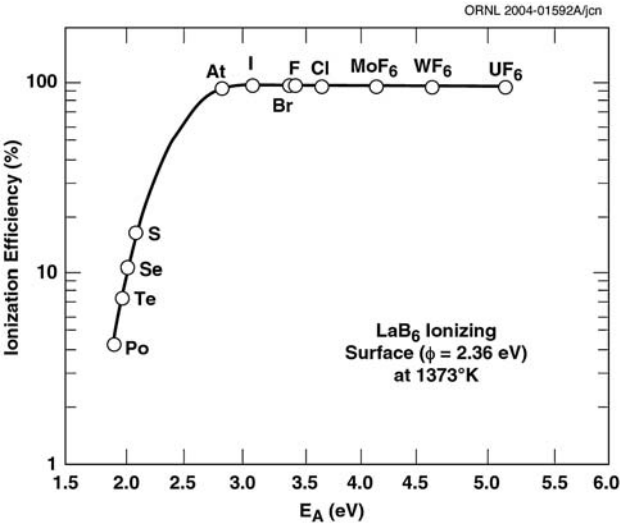

Fig. 12.7. Calculated ionization efficiency (12.23) versus electron affinity E_{A} of selected elemental and molecular species

12.6.2 Negative-Surface-Ionization Sources

Surface ionization can be used to great advantage for radioactive-ion-beam (RIB) applications to eliminate isobaric contaminants that may compromise experimental results with these beams, because of its highly chemically selective character. Ion sources based on the surface ionization principle are generally characterized by a high degree of ion beam purity (chemical selectivity), a limited range of species capability and excellent beam quality (low emittance). The energy spreads are typically of the order of thermal energies ($\sim 2kT \ll 1\,\mathrm{eV}$). The efficiency for negative-ion formation can be high or low, depending on the electron affinity of the species in relation to the work function of the ionizing surface. However, negative surface ionization has not been utilized frequently for generation of negative-ion beams – principally owing to the lack of chemically stable low-work-function materials for use as ionizers, in contradistinction to its positive-surface-ionization counterpart, where several high-work-function metals may be chosen for this purpose.

LaB_6 is usually used for negative surface ionization because of its relatively low work function ($\phi = 2.3$ to $3.2\,\mathrm{eV}$) [69–73] and its availability, despite its widely publicized propensity for poisoning [74, 75]. The poisoning effect is attributable to the interaction of the hot LaB_6 with residual gases in the vacuum system, usually under high-flow-rate conditions or higher-than-optimum-pressure conditions. The effect raises the work function of the LaB_6 surface, thereby reducing the probability of ionizing electronegative atoms as they evaporate from the surface. Under high-flow-rate conditions, the poisoning process also affects the reliability of operation of sources equipped

with this material through-time-varying fluctuations of the ion beam intensity caused by variations in work function [75]. An increase in the work function causes an exponential diminution of the probability for negative-ion formation and, consequently, a reduction in the intensity of extracted negative-ion beams. Despite the poisoning problem, sources based on the use of LaB_6 ionizers have been described in the literature [75–78], including their use at ISOL facilities for negative-ion generation of high-electron-affinity radioactive species [77, 78]. A cross-sectional side view of the source described in [75], equipped with a spherical-sector LaB_6 ionizer, is displayed in Fig. 12.8. Ionization occurs whenever highly electronegative atoms/molecules fed into the source strike the spherical-sector ionizer. Negative ions so formed are accelerated by the converging optics of the negatively biased spherical sector extraction system and focused through the ion emission aperture.

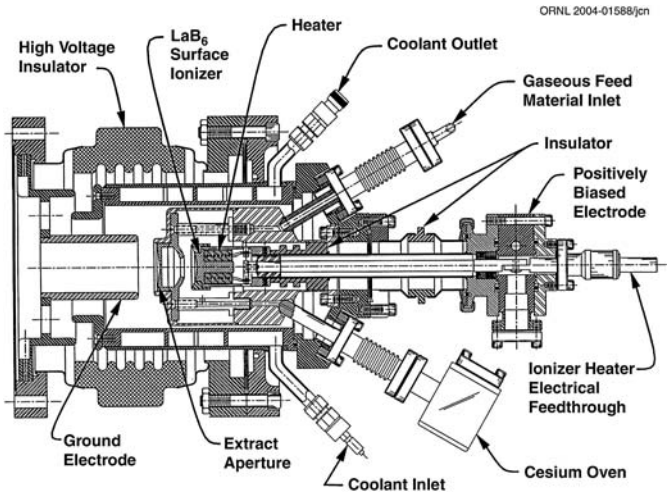

Fig. 12.8. The self-extracting negative-surface-ionization source described in [75], equipped with a spherical-sector LaB_6 ionizer

12.7 Secondary Negative-Ion Formation Processes: Nonthermodynamic-Equilibrium Surface Ionization

Since its discovery [79], the technique of sputtering a surface covered with a fractional layer of a highly electropositive adsorbate such as Cs has proved to be close to a universal method for generating atomic or molecular negative-ion beams from chemically active elements. Sputtering is generally caused by a cascade of momentum transfer processes between recoil atoms initially set in motion by an energetic projectile that leads to ejection of surface atoms.

The process is measured in terms of the sputter ratio, or yield per incident particle, S. In contradistinction to the process of conventional surface ionization, it is a nonthermodynamic equilibrium process and thus differs from thermal evaporation. For more details on the mechanisms involved in sputtering, and tabulated yield data for a variety of projectile–target interactions, early reports can be found in [80–83].

Although several independent and distinct negative-ion formation processes may coexist during sputtering, particularly from compound and alloyed samples, there is a preponderance of evidence that the mechanism of negative-ion formation during sputtering of "clean" metal surfaces with a low coverage of a highly electropositive adsorbate, such as one of the group IA elements, is a form of surface ionization. The practical implementation of the technique as a source of negative ions is quite simple, as illustrated schematically in Fig. 12.9. Positive-ion beams, formed either by direct surface ionization of a group IA element or in a Cs-rich noble-gas plasma discharge (Ar, Kr or Xe), are accelerated to between a few hundred eV and several keV, where they sputter a sample containing the element of interest. A fraction of the sputtered particles leave a negatively biased sample containing the species of interest as negative ions and are accelerated through an aperture in the source.

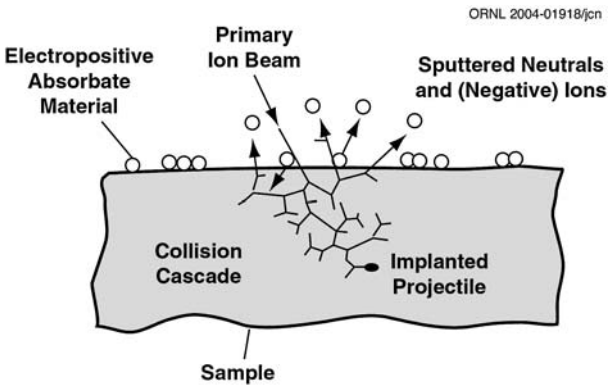

Fig. 12.9. Illustration of negative ion formation by energetic particle bombardment of a metal covered with a fractional layer of a highly electropositive adsorbate

12.7.1 Negative-Ion Sources Based on the Sputter Principle

Negative-ion source technology has steadily advanced over the years, in keeping with the continual demand for higher-intensity negative-ion beams with improved beam quality for a variety of tandem-electrostatic-accelerator-based fundamental and applied research. Heavy-negative-ion sources have been developed that utilize Cs surface ionization sources separated in space from the

sputter sample. In such sources, the energetic Cs^+ beams both sputter and lower the work function of the surface. The effect of the Cs on the work function varies from to sample to sample because of differences in the saturation value for implanted Cs in the particular material surface. Thus it is difficult to achieve optimally low-work-function surfaces and consequently maximum negative-ion yields in this source type. This problem was subsequently overcome in the next-generation plasma-sputter and Cs-sputter negative-ion sources by directly feeding Cs vapor from an external oven at a controlled rate into a chamber containing a negatively biased sample probe and a means for producing positive-ion beams for bombarding samples containing the species of interest.

Plasma-sputter sources utilize either filaments or RF antennae for generating plasmas from which positive ions are extracted for sputtering the material of interest, while Cs-sputter negative-ion sources utilize hot surface ionizers for producing Cs^+ beams for this purpose. Sources based on this principle offer near-optimum conditions for generating negative-ion beams. These sources are said to be self-extracting in that negative-ion beams are accelerated from a negatively biased sputter probe within the plasma volume through an extraction aperture in the source. In addition to being versatile in terms of species, sources based on this concept are simple in design and easy to operate, and generally have long lifetimes. Because of these factors, heavy-negative-ion sources based on the sputter principle are utilized extensively in tandem electrostatic-accelerator laboratories.

Cs-Sputter Heavy-Negative-Ion Sources Equipped with Porous-W Surface Ionizers

The Müller and Hortig Negative-Ion Source

Through evolutionary processes, several types of heavy-negative-ion sources have been developed over the years since the discovery by Krohn that negative-ion yields are greatly enhanced by the presence of a thin layer of a highly electropositive alkali metal on the material being sputtered [79]. The first source to utilize the sputter principle was developed by Müller and Hortig [84]. The source utilized a continuously rotating wheel made of the material of interest, onto which was evaporated Cs metal vapor at a position diametrically opposed to the ion bombardment position. The sample wheel was bombarded with a 20 keV Ar^+ beam impinging at 20° with respect to the sample surface. Negative-ion beams were then extracted from the area of bombardment with an electrode system positioned perpendicular to the sample wheel. A simplified version of the source with improved performance characteristics was later developed [85]. A top view of the latter source is displayed in Fig. 12.10. Improvements to the source included the replacement of the Ar^+ source with a Cs surface ionization source of the porous-W type. This feature simplified source operation and eliminated the

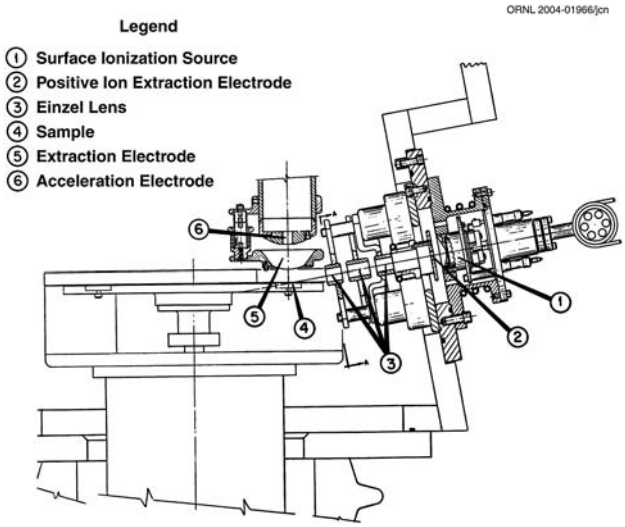

Fig. 12.10. A modified Müller and Hortig negative-ion source equipped with a Cs surface ion source and an asymmetric einzel lens for focusing Cs beams onto sputter samples [85]

necessity of using an external Cs oven. The Cs^+ beam served both to sputter the material and to lower the work function of the surface. In addition, the source incorporated an asymmetrical lens to focus 20 keV Cs^+ beams onto the rotating-wheel sample surface, thereby reducing the asymmetry of the beam spot while increasing the negative-ion beam intensity and reducing the emittance of extracted beams. Although these sources were cumbersome in design, they clearly demonstrated the viability of the technique as means of generating useful beam intensities of a wide variety of species for research, including 25 μA C^-, 30 μA O^-, 40 μA F^-, 20 μA C_2^-, 0.2 μA Al^-, 44 μA S^-, 100 μA Cl^-, 3 μA AlO^-, 1 μA Cr^-, 6 μA Cu^-, 0.8 μA FeO^-, 14 μA Ag^-, 26 μA I^-, 5 μA InO^-, 4.6 μA TaO_2^-, 3 μA Pt^-, and 0.5 μA PbO_2^-.

The Middleton–Adams Source

The next generation of sources based on this technique was that of the Middleton and Adams Cs-sputter negative-ion source, illustrated schematically in Fig. 12.11 [86]. In this source, Cs^+ beams are produced by diffusing Cs vapor through a hot, porous-W ionizer (with a porosity such that $\rho = 0.8\,\rho_0$, where ρ_0 is the density of solid W.). Surface ionization sources generate space-charge-limited beams (several hundred μA up to a few mA) and therefore proper attention must be given to the electrode system design. The effects of space-charge on the sizes and angular distributions of 20 keV Cs^+ beams extracted from a surface ionization source with properly designed electrodes are illustrated in the simulations displayed in Fig. 12.12. The Cs^+ beams are

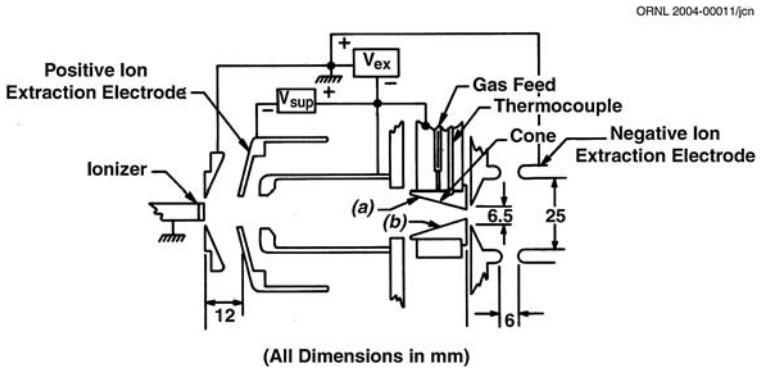

Fig. 12.11. The Middleton–Adams Cs-sputter negative-ion source [86]. The source is equipped with a Cs surface ionization source for producing a Cs^+ beam used to sputter conical-geometry samples

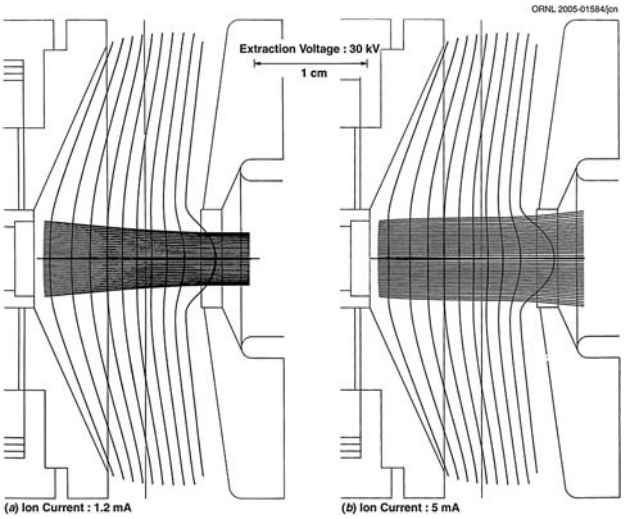

Fig. 12.12. Simulation of Cs^+ beam extraction from a Cs surface ionization source equipped with a porous-W ionizer, illustrating the influence of space-charge on beam trajectories during extraction. Surface ionization sources of this type are utilized in Middleton–Adams and refocus geometry Cs-sputter negative-ion sources. Extraction voltage $V_{ex} = 20\,\mathrm{kV}$. Ion current (**a**) 1.2 mA; (**b**) 5 mA

accelerated to 20 keV and used to bombard the inner surface of a conical bore (half-angle 20°) in the material of interest. The Cs^+ beam serves to sputter the material of interest as well as to lower the work function of the sample surface. Negative ions are extracted at 20 keV through a 3 mm diameter hole bored into the apex of the sample. The ion optics of the negative-ion extraction region of this source are illustrated in Fig. 12.13. Because of the electrode

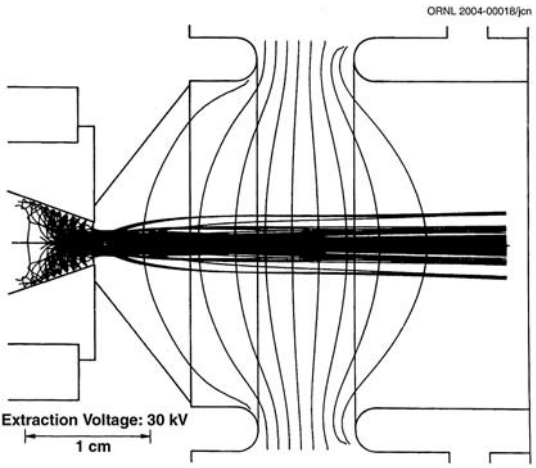

Fig. 12.13. Simulation of extraction from the Middleton–Adams or refocus-geometry Cs-sputter negative-ion source

configuration, the method of extraction and the intrinsically high energy distributions of the sputter process, negative-ion beams have high aberration coefficients and, consequently, have relatively large emittances. Because of the simplicity, reliability, versatility and long lifetime of this source type, it was quickly adopted for use in many tandem accelerator laboratories. The Middleton–Adams source was subsequently improved by introducing a lens–steerer combination between the Cs surface ionization source and the conical targets [87]. The modified source is often referred to as the refocus-geometry Cs-sputter negative-ion source.

The Inverted Cs-Sputter Negative-Ion Source

A Cs-sputter negative-ion source similar in principle to the Middleton–Adams source was developed by Chapman [88], with the exception that the sample and ionizer are reversed in position. A side view of the source is schematically displayed in Fig. 12.14. This source also utilizes samples with a conical taper in the region of ion generation that are attached to an indexable (rotatable) multisample wheel that can be loaded through an access port prior to source operation. The objective of this development was to improve the emittance and brightness of the original Middleton–Adams source while simultaneously solving the chronic ionizer erosion problems attributable to backstreaming of heavy negative ions, generated at the conical sample and accelerated back along the axis of the source to the ionizer. The Cs^+ beams are generated by diffusion through a annular, porous-W surface ionizer surrounding a central hole, through which sputter-generated negative ions pass during extraction. The species capabilities of the inverted source are similar to those of the original and refocus-geometry versions of the Middleton–Adams source. However,

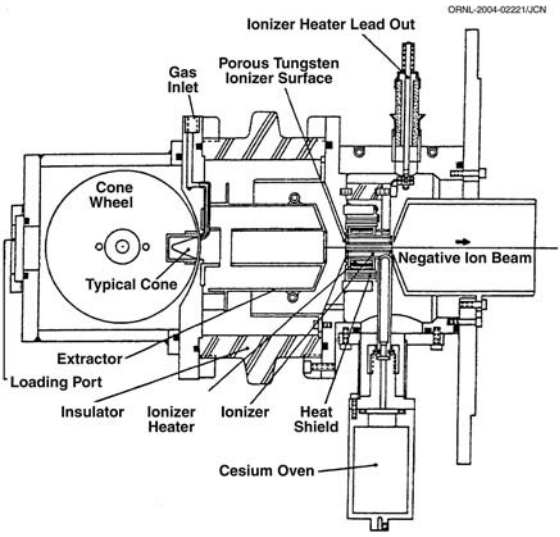

Fig. 12.14. Side view of the inverted Cs-sputter negative-ion source

because of the rather long extraction canal through the annular ionizer, extracted beam intensities from the inverted source are lower than those for the respective Middleton–Adams versions.

The ORNL KENIS Source for ISOL Radioactive-Ion-Beam Generation

Chemically active radioactive species are often released from target materials in a variety of molecular forms. For example, ^{17}F is principally released from an Al_2O_3 target material as $Al^{17}F$. Because of the low probability of simultaneously dissociating such molecular carriers and efficiently ionizing their atomic constituents with conventional hot-cathode, electron-impact ion sources, the species of interest are often distributed in several mass channels in the form of molecular sideband beams. Consequently, the beam intensities of the desired radioactive species are diluted. The sputter negative-ion beam generation technique is particularly effective for simultaneously dissociating molecular carriers and efficiently ionizing highly electronegative atomic constituents. Therefore, a new-concept kinetic-ejection negative-ion source (KENIS), based on this principle, was conceived to address this problem [89]. Because of geometric considerations associated with the scheme used at the Holifield Radioactive Ion Beam Facility (HRIBF) [90], the Middleton–Adams source geometry is best suited for this particular application. A three-dimensional representation of the source is displayed in Fig. 12.15, and a side view of the details of the ionization region of the source is shown in Fig. 12.16. Radioactive species, formed through fusion–evaporation nuclear reactions in a hot target irradiated with high-energy beams of either H^+,

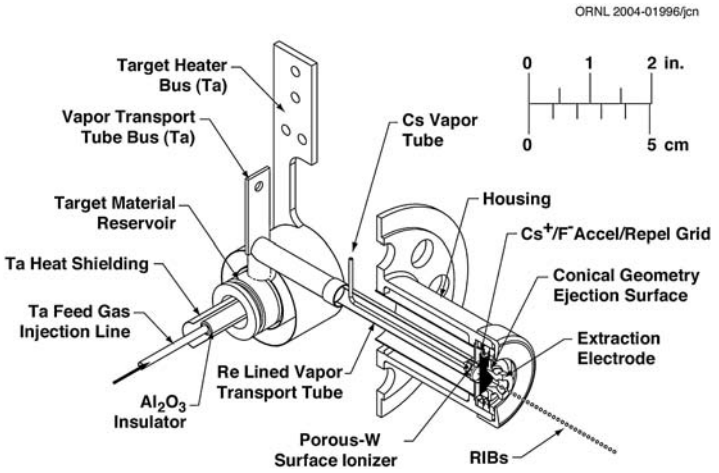

Fig. 12.15. Isometric cutaway drawing of the kinetic-ejection negative-ion source (KENIS) utilized for radioactive-ion-beam generation at the Holifield Radioactive Ion Beam Facility (HRIBF)

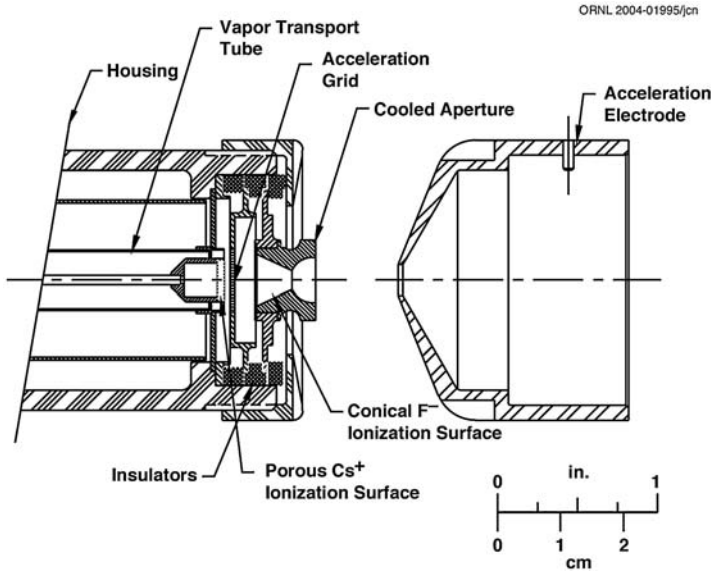

Fig. 12.16. Side view of the negative-ion generation region of the kinetic-ejection negative-ion source (KENIS) showing the porous-W Cs surface ionizer, the acceleration grid and the conical-geometry cathode where negative ions are formed

D^+ or $^{3,4}He^{++}$, are released through diffusion from thin-fiber target materials and transported to the ionization region of the source, where they are adsorbed onto a conical surface bored into a Ta cathode. Radioactive particles that collide with the cathode are bombarded with ∼200 eV Cs^+ beams produced with a porous-W ionizer. Negative ions are sputter-ejected and extracted through a 2 mm hole bored into the apex of the cone. The source is equipped with a negatively biased grid for repelling negative ions that are ejected rearward (i.e., toward the Cs surface ionization region of the source) and would be otherwise lost. The source has proven to be highly efficient for simultaneously dissociating AlF carrier molecules and forming atomic F. The source has been successfully employed on-line to generate high-intensity $^{17,18}F$ beams for astrophysics research at the HRIBF (using the $^{16}O(d, n)^{17}F$ reaction).

Cs-Sputter Heavy-Negative-Ion Sources with External Cs Ovens

Early negative-ion source developments in the respective forms of the Müller–Hortig [84, 85], Middleton–Adams [86], refocus-geometry [87] and inverted-geometry [88] negative-ion sources clearly demonstrated their reliability, long lifetime and versatility for generating useful beam intensities of a wide variety of negative-ion species. However, the use of a surface ionization source to both generate Cs^+ beams for sputtering and simultaneously lower the work functions of sample surfaces is typically nonoptimum for the realization of maximum negative-ion beam intensities, particularly for high-sputter-ratio samples, and the extraction geometries were generally incompatible with the lowest practically achievable emittances. Following the successful development of the radial-geometry plasma-sputter source ANIS at the University of Aarhus, described below, a generation of axial-geometry sources evolved which borrowed certain features of the ANIS, including an external oven for feeding Cs vapor at a controlled rate into a chamber that houses a negatively biased probe containing the material of interest. These sources are self-extracting, and therefore the emission boundaries can be designed to ensure minimum losses during beam transport to the extraction aperture. Several sources of this type have been developed at a variety of laboratories, including those described in [91–93]. In these sources, the negatively biased sputter samples are placed in a cesium-rich environment, where they are sputtered with Cs^+ beams produced by Cs vapor in direct contact with a hot surface ionizer. The sources differ only in the geometry of the positive-ion surface ionizer, its spacing in relation to the negatively biased sample, the spacing of the sample in relation to the ion exit aperture, and the aperture size. The electrode geometry in this source type determines the optical properties of the cesium-ion beam. The perveance P of the system and the shape of the ionizer form an electrode system which determine the perveance for Cs^+ beams and therefore the magnitude of the space-charge-limited currents at a given extraction voltage. The shapes of the electrodes determine

the positive transport optics as well as the distribution of the current at impact with the sample. The positive-ion distribution, in turn, determines the shape and distribution of the negative-ion beams produced in a particular source. Since the particle speeds are lowest as they leave the sample surface, it is very important to contour the surface so that a high percentage of the sputter-ejected beams are transported back through the extraction aperture of the source. The codes described in [35–40] are extremely accurate and are valuable, cost-effective resources for quickly arriving at optimized electrode systems, as well as for simulating the beam transport optics of both positive- and negative-ion beams. Through their use, the geometry of the ionizer/negative-ion-generation electrode system can then be designed to produce the highest practically achievable negative-ion beam intensities (e.g. to optimize the perveance for Cs^+ beam generation and thereby maximize the negative-ion yields while reducing the emittance to the lowest achievable value for the source). Several single-sample axial-geometry sources, equipped with an external oven for feeding Cs vapor into a vacuum chamber housing a surface ionizer and a sputter cathode made of the material of interest, have been developed for use at a variety of laboratories, including sources equipped with cylindrical-geometry [93–98], spherical-geometry [98–104], ellipsoidal-geometry [103,104] and conical-geometry ionizers [92,105], among which are sources equipped with remotely indexable sputter samples [99–102,105].

Source of Negative Ions by Cesium Sputtering (SNICs)

Following the successful radial-geometry plasma-sputter negative-ion source developments embodied in the ANIS, discussed below, a negative-ion source referred to as SNICS was developed at the University of Wisconsin [93]. This source was the first of a series of very successful axial-geometry Cs-sputter negative-ion sources that were equipped with an external oven for introducing Cs into the chamber and with means for producing Cs^+ beams for bombarding a negatively biased sputter probe containing the material of interest. A schematic representation of the source and the potential arrangement is shown in Fig. 12.17. The SNICS source utilizes a cylindrical-geometry, spiral-wound W filament for producing Cs^+ beams; these beams are accelerated to a negatively biased, concave, spherical-geometry cathode placed an optimum distance away from the ionizer. The concave spherical surface provides some focusing action on negative-ion beams during transport that helps to limit the angular excursion of extracted beams. Because of the spiral-wound filament and the cylindrical geometry of the ionization surfaces from which Cs^+ is accelerated, the wear patterns on cathodes are very complex. The observed wear pattern from this source is composed of two parts: a region of concentrated wear with a full diameter of $\sim$1 mm, surrounded by a strongly graded halo region that extends out to the diameter of the cathode, depending on the position of the cathode relative to the ionizer. Thus, negative-ion beams extracted from the source have a complex distribution that affects

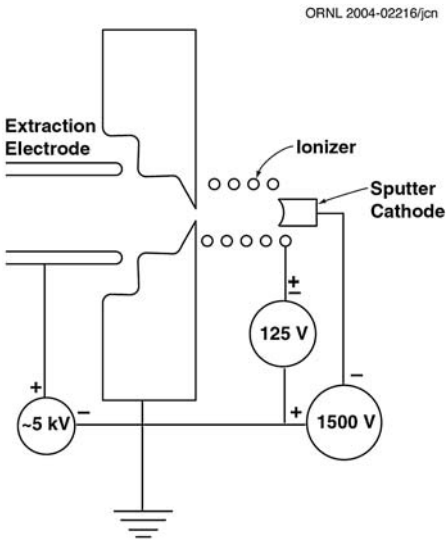

Fig. 12.17. Schematic representation of the Source of Negative Ions by Cesium Sputtering (SNICS), and potential arrangement

their emittance. During initial testing, the source was operated with Cu^- beams at intensities up to 38 μA.

Source Equipped with a Conical-Geometry Ionizer

A cesium-sputter negative-ion source equipped with a conical-geometry ionizer [92,105] will serve to illustrate the principles of this source type. A cross-sectional side view of the single-sample version of the source is displayed in Fig. 12.18. The negative-ion yields are maximum at a specific Cs oven temperature, which typically is found to be independent of the species of interest. Once the oven temperature is determined, the value is usually fixed during operation of the source and never exceeded. The simplest and best method for control of beam intensity is by adjustment of the cathode sputter voltage to the desired value. Negative-ion-beam intensities versus sputter probe voltage also exhibit maxima that typically depend on the Cs oven temperature. It is also important to know the relation between Cs^+ current and sputter probe voltage, as the positive-ion current dictates the rate of sputtering. The perveance P of the electrode system for Cs^+ is 4.3×10^{-9} A/V$^{3/2}$. Trajectories of Cs^+ ions flowing through the electrode structure under space-charge-limited conditions, computed with the code described in [38], are shown in Fig. 12.19. The computed ion current density resulting from positive-ion impact at the sample surface is distributed over a full diameter of 6 mm. This feature is desirable for potential use for generating radioactive ion beams, where good overlap between the condensed vapors and the cesium ion beam

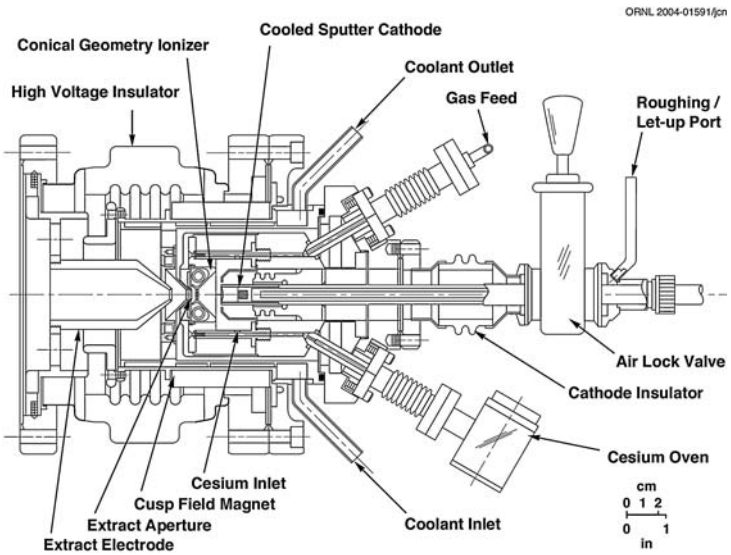

Fig. 12.18. Side view of the Cs-sputter negative-ion source equipped with a conical-geometry surface ionizer developed at the Holifield Radioactive Ion Beam Facility for stable negative-ion-beam generation

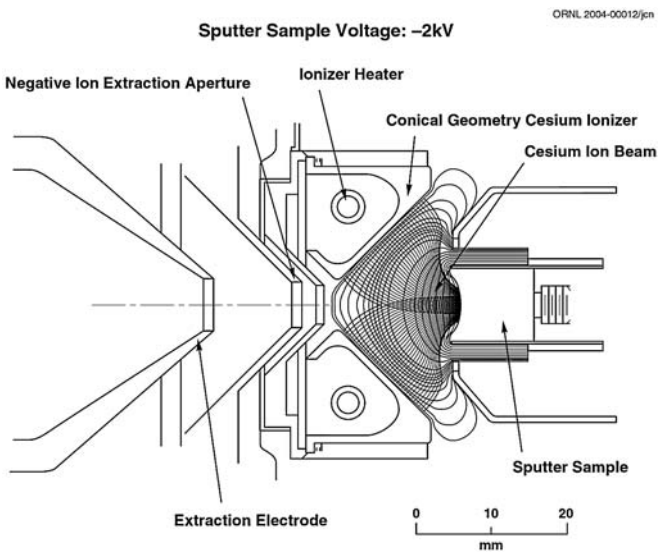

Fig. 12.19. Cs^+ beam optics of the Cs-sputter negative-ion source equipped with a conical-geometry surface ionizer

is required. An example of negative-ion trajectories flowing countercurrent to the positive-ion beam through the electrode system is shown in Fig. 12.20. These calculations were also performed with the code described in [38]. The negative-ion beam current density at the sample surface is assumed to mimic that of the positive-ion current density distribution. The influence of the positive-ion beam space charge on the negative-ion beam is included in the simulations.

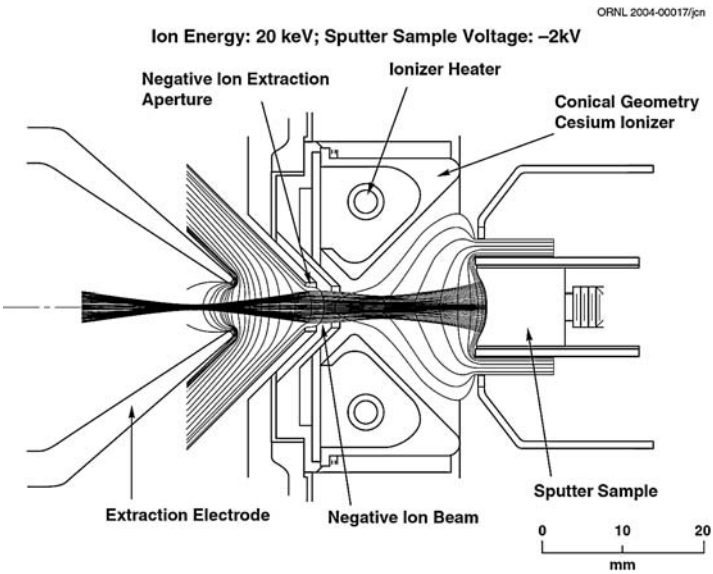

Fig. 12.20. Negative-ion beam optics of Cs-sputter negative-ion source equipped with a conical-geometry surface ionizer

Source Equipped with a Cylindrical-Geometry Ionizer

A source equipped with a solid-W cylindrical ionizer was developed at the Oak Ridge National Laboratory [95, 96]. The ionization chamber and details of the ionizer and sputter probe electrode configuration for the source are shown in Fig. 12.21. The computed cesium current density distribution and observed sample wear pattern agree remarkably well for this source. The observed wear pattern is composed of two parts: a region of concentrated wear pattern with a full diameter of ~ 0.75 mm, surrounded by a low-density halo region that is uniformly worn over a diameter of ~ 4.5 mm. Thus, beams extracted from the source have two different characters: (1) a high-density beam located on axis, and (2) a uniformly distributed halo beam surrounding the high-density central region. Thus, both beams contribute to the emittance of the source with this ionizer geometry. Although the Cs^+ ion current versus

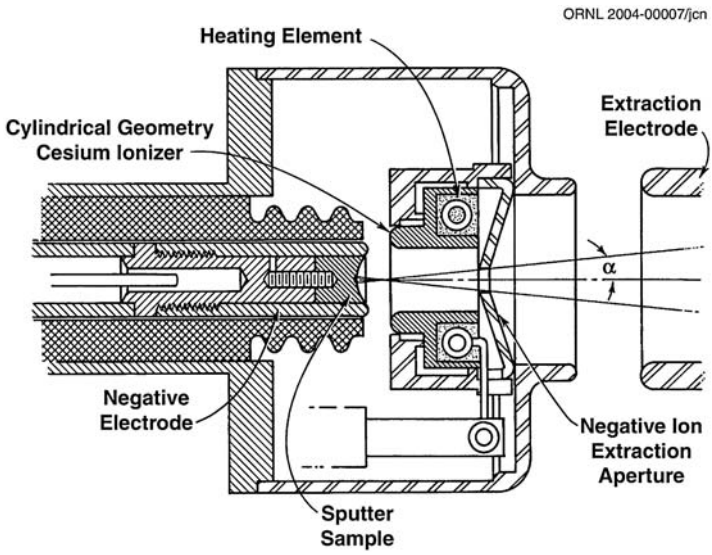

Fig. 12.21. Schematic drawing of the ion formation and extraction region of the Cs-sputter negative-ion source equipped with a smooth-surface, cylindrical-geometry W surface ionizer

sputter probe voltage for this electrode system has not been measured, according to calculations made with the code described in [35], the perveance for Cs^+ beams is very high ($P \cong 57 \times 10^{-9}\,A/V^{3/2}$).

The Model 860 Cs-Sputter Negative-Ion Source Equipped with a Spiral-Wound Ta Ionizer

The type and geometry of the Cs surface ionizer and its position relative to the sputter cathode affect the positive-ion distribution at impact and, consequently, the negative-ion distribution, since the negative-ion distribution leaving the surface mimics that of the positive-ion beam. Hence, the quality of the negative-ion beam depends on the geometry of the ionizer/sputter probe electrode system. The wear pattern on the cathode determines to first order the distribution of the positive-ion beam in these sources. Codes such as those described in [35–40] predict with remarkable accuracy the observed wear patterns in these sources. A side view of the ionization region of the Model 860 source [97] is displayed in Fig. 12.22. The observed wear patterns on sputter cathodes mounted in a source equipped with a spiral-wound ionizer are found to be more complex than in those equipped with ionizers of other geometries. Typically, the central region of the cathode is found to be strongly worn, within a diameter of ∼1 mm surrounded by a larger-diameter ($\phi \cong 8$ mm), asymmetrically distributed halo region. The asymmetrical wear pattern within the halo region is attributable to the spiral character of the

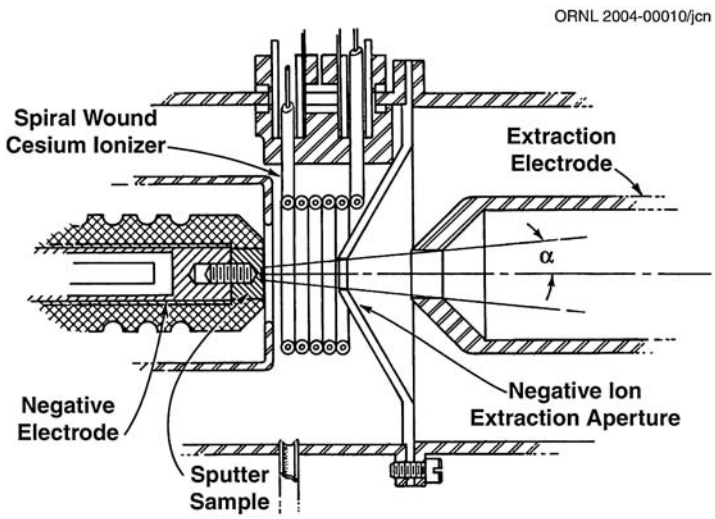

Fig. 12.22. The ion formation and extraction region of the Model 860 negative-ion source equipped with a spiral-wound Ta surface ionizer

Ta ionizer. The presence of the large halo beam, as is the case for the source equipped with a smooth-surface cylindrical-geometry ionizer [95, 96], contributes to the emittance of the source. The perveance of this electrode system has not been measured but is estimated to be $P \sim 60 \times 10^{-9}\,\mathrm{A/V^{3/2}}$.

Source Equipped with a Spherical-Geometry Ionizer

Sources have also been developed at the Oak Ridge National Laboratory that utilize spherical-geometry ionizers [98, 99]. The ionization chamber and ionizer sputter probe arrangement for a single-sample source equipped with a spherical-geometry ionizer [98] are illustrated schematically in Fig. 12.23. According to computational studies and experimental measurements, when the sputter probe is optimally positioned at the focal point of the ionizer, the positive-ion current density distribution at impact with the sample surface is ∼0.75 mm in diameter. This particular ionizer does not exhibit a halo surrounding the central high-density distribution. Therefore the central region of the distribution serves as the sole source from which negative-ion beams are generated. According to computational analyses, with the code described in [35], the perveance for Cs^+ beams for this electrode geometry is $P \cong 2 \times 10^{-9}\,\mathrm{A/V^{3/2}}$.

Source Equipped with an Ellipsoidal-Geometry Ionizer

The ionization region of a single-sample source equipped with an ellipsoidal-geometry ionizer is shown in Fig. 12.24. The source has been briefly described in [103, 104]. When the sputter sample is placed at the focal point of the

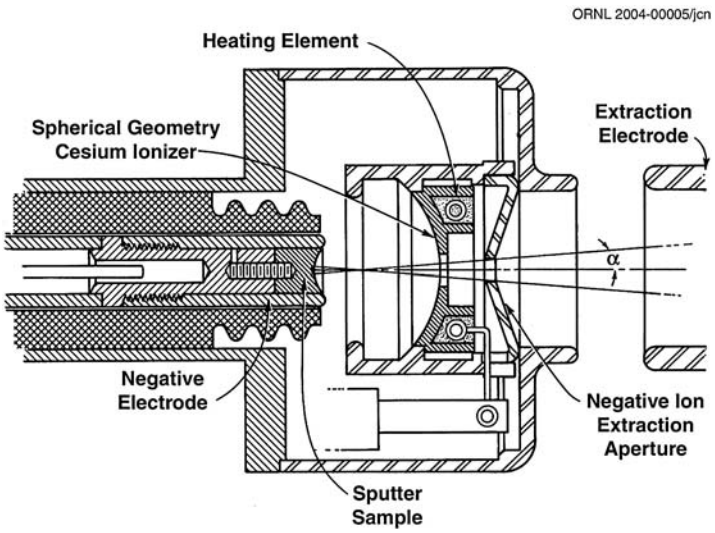

Fig. 12.23. The ion formation and extraction region of a Cs-sputter negative-ion source equipped with a spherical-sector-geometry surface ionizer

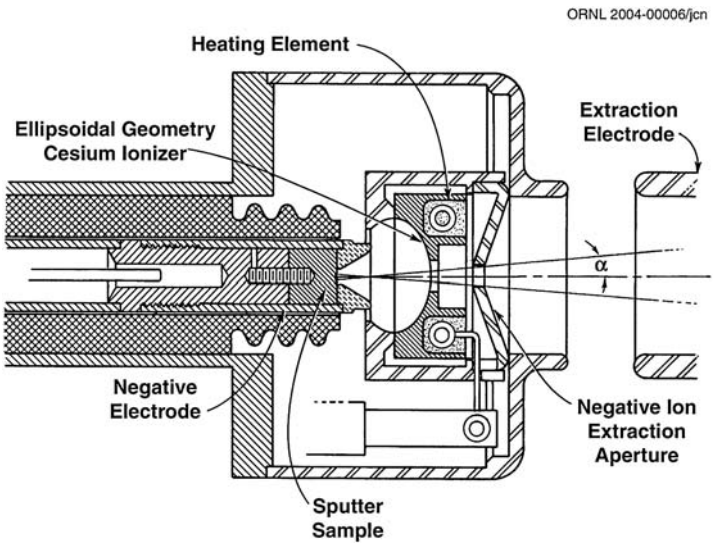

Fig. 12.24. The ion formation and extraction region of a Cs-sputter negative-ion source equipped with an ellipsoidal-geometry surface ionizer

system, the wear pattern at impact has $\phi \cong 1.25$ mm. This geometry has a high perveance in relation to other ionizer geometries with focusing attributes. According to calculations with the code described in [35], the source has a high perveance for Cs^+ beam formation of $P \sim 17 \times 10^{-9}\,\mathrm{A/V^{3/2}}$.

Multiple-Sample Sources

For applications where both high efficiency and/or high-frequency sample changes are desirable, as for accelerator mass spectrometry (AMS) applications, the ability to process multiple samples is essential. A few sources have been designed that meet this requirement, including the sources described in [99–102, 105]. A close-up of the multiple-sample source described in [105] is shown in Fig. 12.25. The source is equipped with a conical-geometry ionizer and a remotely controlled, eight-sample, wheel-type sample-indexing mechanism. The source described in [99] has a 60-sample, wheel-type computer-controlled indexing mechanism.

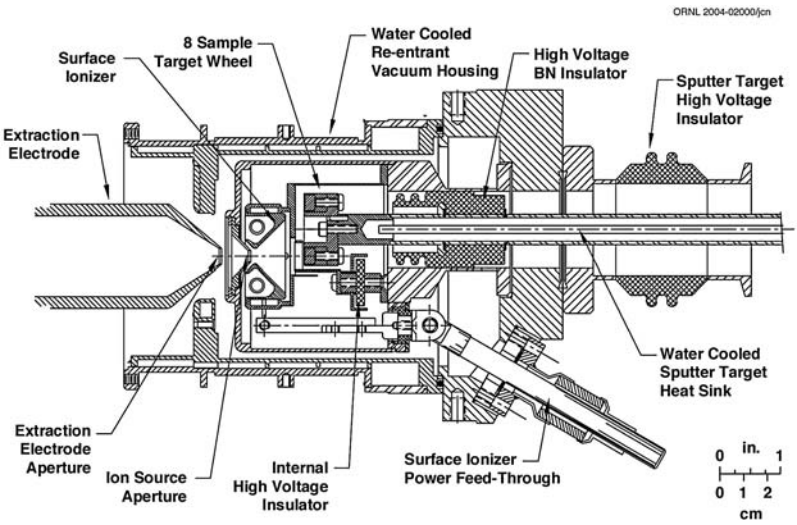

Fig. 12.25. Top-view cross section of the multisample Cs-sputter negative-ion source, equipped with a conical-geometry surface ionizer [105], that was developed for batch mode generation of radioactive ion beams at the Holifield Radioactive Ion Beam Facility

Negative-Ion-Beam Intensity Data

The negative-ion beam intensities that can be extracted from the sources previously described depend on a number of factors. The sputtering rate depends on the sample material, the magnitude of the cesium ion current and the cesium ion energy used to sputter the sample material, and these, in turn, depend on the source operational parameters, for example the cesium oven temperature and the sputter probe voltage. The space-charge-limited cesium current I^+ that can be accelerated at a given sputter probe voltage V and subsequently used for sputtering the sample depends on the perveance P of

the particular electrode configuration. The negative-ion current which can be extracted from the total current generated in the sputter process depends on the electron affinity of the species of interest, the work function of the surface, the size of the negative-ion generation region on the sample surface, the angular distribution of the negative-ion current at the ion-extraction aperture, the spacing of the sample in relation to the aperture, the aperture size and the sputter probe voltage V. Because of operational variables and the differences in the ionizer/sample electrode configuration, the negative-ion currents for a particular species will, in general, differ from source to source, and for a particular source, will vary from one operational period to another. Negative-ion yields for a particular species will depend on the chemical composition of the sample as well. The versatility of the sources described above is reflected by the wide spectrum of momentum-analyzed negative-ion beams that have been observed during their operation.

Atomic negative beams cannot be formed for elements with negative electron affinities, and elements with very low positive electron affinities often cannot be produced with intensities adequate for research. However, the chemically active elements can often be synthesized in situ by introducing appropriate chemically active gases into the ionization chamber of the source at a controlled rate. The gases react with the sputter cathode material to form molecular hydrides, carbides, oxides or halides with sufficiently high electron affinities to produce useful molecular beams containing the element of interest. The element of interest is released by accelerating the molecular beam to high energy in a tandem electrostatic accelerator, where the molecular carrier is dissociated and the atomic species are stripped to form high positive charge states in the terminal of the machine. Improved methods for producing beams of difficult elements such as the group IA elements have been reported in the literature. For example, Alton and Benjamin have developed an improved method for generating negative hydride beams of the group IIA elements [106] based on the use of composite cathodes, and Alton and Mills have developed a new method for generating beams of the group IA elements from metal carbonates [107]. Middleton and Alton have independently evaluated many solid and powder elemental, metal carbide, metal oxide, metal halide, metal carbonate, and composite-mixture cathodes, as well as techniques for in-situ syntheses of chemical compounds containing the species of interest during the sputter process. From these efforts, the best methods for forming useful beam intensities of most species have been developed. Middleton has tabulated the results of studies designed to determine the best cathode material for generating useful beams of almost every chemically active element [108].

Emittance Data

Emittance and brightness measurements for sources equipped with spherical-geometry, ellipsoidal-geometry and cylindrical-geometry ionizers, as well as

for the Model 860 source, have been reported previously [103, 109, 110]. The average normalized emittance versus the percentage of negative-ion-beam intensity contained within a given contour for these sources, as well as that for a source equipped with a conical-geometry ionizer [92, 105], are displayed in Fig. 12.26. In these sources, the geometry of the ionizer/sputter sample system electrode determines the size and shape of the cesium ion beam at impact with the surface. For small sample sizes, a focusing-geometry electrode system may be desirable. As indicated in Fig. 12.26, the emittances of negative-ion beams extracted from sources equipped with electrode systems that focus the cesium beam on the sample surface are somewhat lower. The conical-geometry source has the lowest emittance, while that of the Model 860 is considerably larger than for those equipped with the other ionizer geometries, principally owing to the increased size of the exit aperture used in this source.

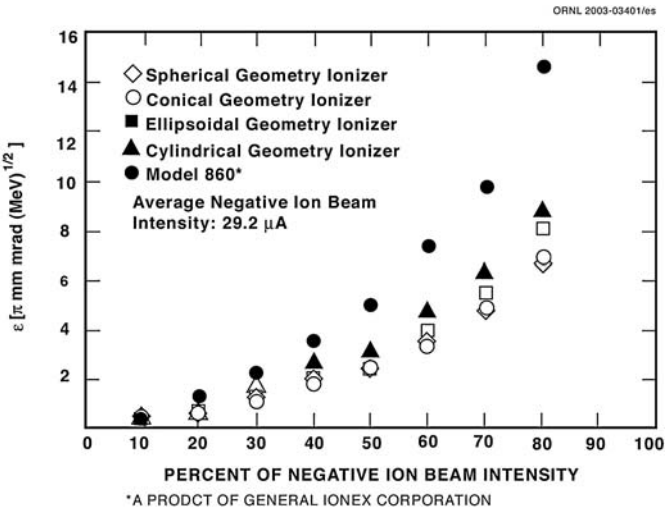

Fig. 12.26. Normalized emittance versus percentage of negative-ion-beam intensity for Cs-sputter negative-ion sources, equipped with cylindrical, spherical-sector, ellipsoidal and conical-geometry ionizers, developed at the Holifield Radioactive Ion Beam Facility, and for the Model 860 negative-ion source

Plasma-Sputter Heavy-Negative-Ion Sources

The advent of Cs-seeded plasma-sputter heavy-negative-ion sources has significantly advanced the state-of-the-art of heavy-negative-ion source technology. Several sources have been developed since the successful development of the radial-geometry University of Aarhus negative-ion source (ANIS)

[111,112], including those described in [113–115,120–126]. In this source type, negative ions, created in the sputter process, are accelerated across a double-layer plasma sheath that surrounds and exactly conforms to the shape of negatively biased spherical- or cylindrical-geometry sputter probes. In later developments, the multi-cusp-field plasma-confinement technique makes it possible to effectively confine the plasma while preserving uniform sputtering over variable-size spherical- or cylindrical-sector sputter probes, when operated in a high-density plasma mode, because of the low magnetic-field flux density in the central region of the plasma chamber. Thus, the emission area can be scaled to meet the intensity requirement of a particular experiment. The plasma sheath serves as a lens to focus the beam through the plasma to the ion exit aperture of the source. Since space-charge effects are precisely compensated during passage through the plasma, very high beam intensities can be extracted from this type of source. Thus, high beam intensities can often be realized while preserving a reasonable emittance value. The intensity levels for certain species from plasma-sputter negative-ion sources, such as those described in [120–126], are often higher by factors of 3–100 than those generated in conventional cesium-sputter negative-ion sources, and yet the emittances ε_N of the beams are reasonably small. In sources that use hot cathodes (filaments) to generate the plasma for DC operation, the source lifetime can be limited by sputter erosion of the filament. This problem can, in part, be offset by making provision for filament redundancy or by use of RF plasma generation techniques.

The tandem accelerator has also been either used or considered for use as an injector for synchrotron heavy-ion accelerators. The plasma-sputter negative-ion source is well suited for this application in that pulsed negative-ion beam intensities exceeding the practical value of $\sim$200 μA (peak intensity) can be delivered to the synchrotron from the tandem electrostatic accelerator for a wide variety of heavy-ion species. It also offers the prospect of use for batch-mode generation of radioactive ion beams for injection into tandem electrostatic accelerators for postacceleration, because of the perfect overlap of the plasma particles that sputter the sample and the area of the sample irradiated by the production beam. In general, plasma-sputter negative-ion sources generate higher beam intensities with improved emittances than do their Cs-sputter counterparts. These sources all utilize hot cathodes for plasma ignition, with the exception of the sources described in [115,123,124], which use RF antennae for plasma ignition.

The University of Aarhus Negative-Ion Source (ANIS)

While Cs-sputter source designs that use porous-W surface ionization sources separated in space from the region of negative-ion generation are very versatile in terms of species, this method of Cs^+ beam formation rarely provides optimum cesium-layer surface coverage, critically important for generating maximum negative-ion yields. With this approach, the cesium surface

content is relegated to the saturation value for Cs in the particular material, and the residual neutral surface Cs is thought to be less than optimally distributed. (The saturation value is the amount of cesium left in the surface after the steady state has been achieved.) Since the saturation value varies inversely with sputter ratio, high-sputtering materials (Cu, Ag, Au, etc.) have a low residual cesium content and thus do not produce negative-ion yields in accordance with the magnitudes of their electron affinities. In addition, negative-ion beams have high aberration coefficients because of the shape of the negative-ion generation surface (the inner surface of a conical bore in the material of interest) and require a means for ion extraction from the surface of generation (through a hole bored into the apex of the cone). In 1975, Andersen and Tykesson of the University of Aarhus introduced a radial-geometry Cs-rich plasma-sputter negative-ion source with very high yields from elemental materials, exceeding considerably the yields of those sources that utilize Cs beams to both sputter and simultaneously lower the work functions of sample surfaces [111, 112]. A version of this source was designed and developed at the Oak Ridge National Laboratory (ORNL) [113], as displayed in Fig. 12.27. Neutral Cs is fed into the discharge chamber at a controlled rate from an external oven. Discharge support gases are metered through a leak valve into the source. A weak dipole magnetic field ($\sim$0.0150 T) is used to collimate a primary electron beam produced by thermionic emission from a Ta filament situated at the end of the plasma chamber. Plasmas are ignited by raising the filament to emission temperature and accelerating electrons to energies typically $<$100 eV. The source is equipped with an external oven that permits precise control of the feed rate of Cs into the plasma discharge and thereby provides a means for optimizing the cesium layer thickness on samples undergoing bombardment, as required for maximizing negative-ion yields. Chemically reactive gases may also be introduced into the discharge,

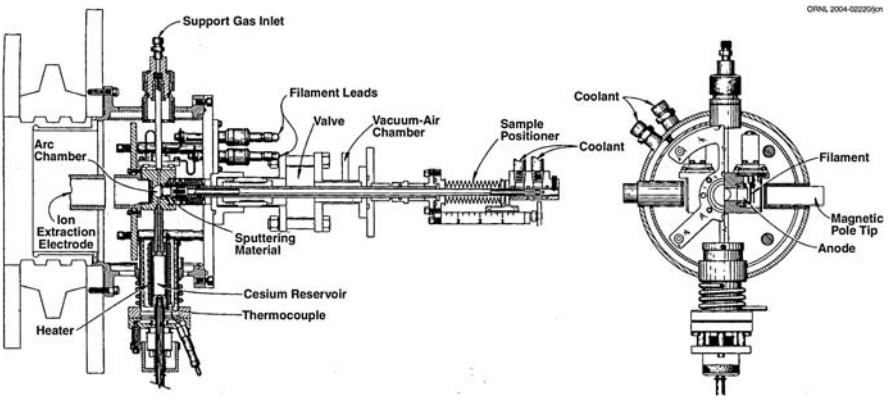

Fig. 12.27. Side and end views of the modified University of Aarhus negative-ion source (ANIS) developed at the Oak Ridge National Laboratory [113]

to react with the cathode material to form intense molecular carrier beams containing the species of interest in cases where the species has a negative electron affinity or the electron affinity is appreciably lower than that of the molecular carrier. Negatively biased samples have concave spherical emission areas that are placed away from the extraction aperture by a distance equivalent to the spherical radius of the sample so that the negative-ion beam is a minimum at the aperture. One of the great advantages of the plasma-sputter source is that the sample surfaces are uniformly bombarded by ions extracted from the plasma sheath, which precisely conforms to the shape of the emission surface. Negative ions are produced by sputtering with energetic positive ions across the plasma sheath that surrounds the spherical-geometry surface. Thus, the plasma sheath acts as a spherical lens that focuses ion beams through the extraction aperture and thus reduces the size of the extraction aperture relative to other emission geometries, thereby restricting losses of neutral Cs from the source. Since the sputter process ejects particles normal to the emission surface, beams created from a concave spherical-geometry surface have lower aberration coefficients than those for other emission geometries. This method of negative-ion generation enables variation of the sputter sample size (diameter and spherical radius) according to the intensity requirements of a particular experiment. The emittances of beams are found to depend on the sputter cathode diameter and the intensity of the species. For a cathode of diameter $\phi = 10\,\text{mm}$, the normalized emittance of a $30\,\mu\text{A}$ C^- beam at the 90% contour level is $\varepsilon_N \cong 1.8\pi\,\text{mm mrad}\,\text{MeV}^{1/2}$ [112]. The beams reported by this group during early characterization studies of the ANIS include $1\,\mu\text{A}$ Li^-, $0.8\,\mu\text{A}$ BeH^-, $3\,\mu\text{A}$ BeO^-, $0.04\,\mu\text{A}$ B^-, $2.5\,\mu\text{A}$ BO^-, $20\,\mu\text{A}$ C^-, $15\,\mu\text{A}$ C_2^-, $5\,\mu\text{A}$ CN^-, $30\,\mu\text{A}$ O^-, $15\,\mu\text{A}$ F^-, $1\,\mu\text{A}$ Al^-, $2\,\mu\text{A}$ Al_2^-, $50\,\mu\text{A}$ Cl^-, $0.9\,\mu\text{A}$ TiH^-, $0.7\,\mu\text{A}$ FeH^-, $6\,\mu\text{A}$ Ni^-, $30\,\mu\text{A}$ Cu^-, $3\,\mu\text{A}$ Ta^-, and $80\,\mu\text{A}$ Au^-. A modified form of the source has been extensively evaluated at the Oak Ridge National Laboratory [113, 114].

The ORNL RF Plasma-Sputter Negative-Ion Source

Filament-ignited sources are limited by the lifetimes of filaments used for plasma ignition because of the erosive nature of the hot-cathode plasma discharge. The use of RF power for plasma ignition, in principle, overcomes this handicap, reduces the complexity of operation and lowers overall source maintenance. However, in practice, sources in which antennae are submerged in the plasma undergo bombardment and, consequently, their lifetimes are also limited by sputter erosion processes. This problem can be ameliorated by antennae coupling RF power through thin-walled glass or ceramic tubes that surround the plasma volume and thus protect the antenna. A compact source based on RF plasma ignition techniques, displayed schematically in Fig. 12.28, has been developed at the Oak Ridge National Laboratory [115]. The main vacuum chamber is equipped with permanent magnets positioned around the periphery of the chamber to form a longitudinal magnetic field

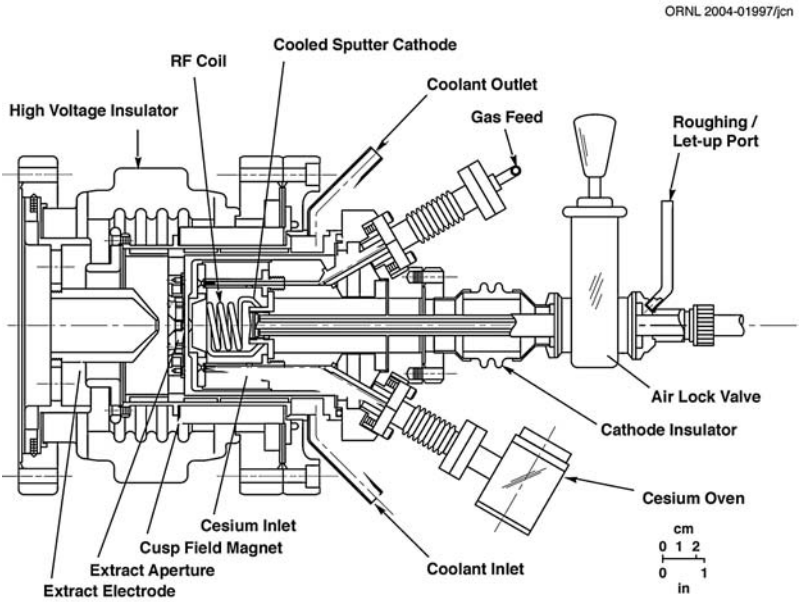

Fig. 12.28. Cross-sectional side view of an axial-geometry RF plasma-sputter negative-ion source [115]

(maximum field strength 0.0380 T) for confinement of the plasma in the radial direction. The source utilizes a porcelain-coated, high-Q, self-igniting, inductively coupled antenna system, operating at 80 MHz, that has been optimized to generate Cs-seeded plasmas at low pressures (typically <100 Pa for Xe). The source can be operated in either pulsed or DC modes for the generation of negative-ion beams. Table 12.5 provides a partial list of momentum-analyzed beams produced by its use. The normalized emittance within the 80% contour for a 200 μA Cu^- beam is $\varepsilon_n \sim 7.5\pi$ mm mrad $(\mathrm{MeV})^{1/2}$. In general, the emittances of this source are lower than those for Cs-sputter sources at the same beam intensity. However, the intensities from the present source and other plasma-sputter negative-ion sources are often considerably higher for a given species.

The KEK Pulsed-Mode, High-Intensity, Plasma-Sputter Negative-Ion Source

The original multi-cusp magnetic-field plasma surface ion source, routinely employed for the production of high-intensity pulsed-mode H^- beams at the LAMPF [116,117] and at the National Laboratory for High Energy Research (KEK) [118,119], has been modified for use as a high-intensity pulsed-mode heavy-negative-ion source [120,121]. A side-view representation of the source is displayed in Fig. 12.29. The developments for heavy-ion production in the case of the KEK negative-ion source are described in [120, 121]. These

Table 12.5. Negative-ion beam intensity data for the ORNL RF plasma-sputter negative-ion source

Ion	Probe Material	Beam Intensity (μA)
C^-	C	610
F^-	LiF	100
Si^-	Si	500
S^-	ZnS	500
P^-	GaP	125
Cl^-	NaCl	200
Ni^-	Ni	150
Cu^-	Cu	230
Ge^-	Ge	125
As^-	GaAs	100
Se^-	CdSe	200
Ag^-	Ag	70
Au^-	Au	250
Pt^-	Pt	125

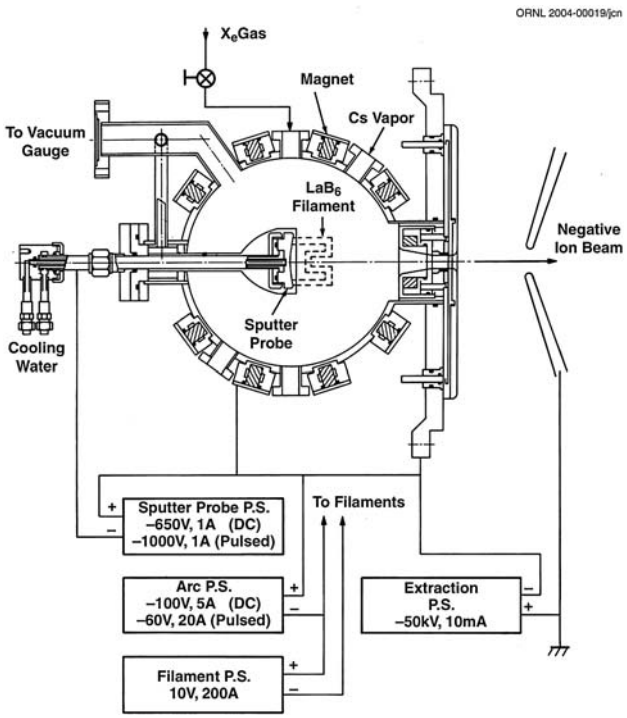

Fig. 12.29. A cross-sectional view of the KEK pulsed-mode, high-intensity plasma-sputter negative-ion source [120, 121]

developments clearly demonstrated the capabilities of this source concept for generating high-intensity (several mA) pulsed negative-ion beams of a wide spectrum of atomic and molecular species. In the original source, the plasma was formed by pulsing the discharge voltage of two series-connected LaB_6 cathodes, thus creating a high-density plasma discharge from Xe feed gas, seeded with cesium vapor, during the discharge cycle. Under pulsed-mode operation at the low duty factors used (typically 2×10^{-3}), the LaB_6 cathodes exhibit very little erosion after many hours of operation. Although principally tested in a low-duty-cycle (repetition rate 1–50 Hz) macropulsed mode (pulse width 50–300 μs) suitable for heavy-ion synchrotron applications, the source can be operated in DC mode and generate heavy-negative-ion beams at mA intensity levels for many atomic and molecular species, including semiconducting-material dopants (B^-, P^-, As^-, Sb^-, etc.), as well as O^- for isolation barrier formation. Since O^- beams are generated from solid materials, chemical reactions between the feed gas and the hot cathodes commonly used in volume-discharge positive-ion sources, which lead to an extremely short cathode lifetime, are avoided. Table 12.6 provides a partial list of total beam intensities (peak), species and probe materials used in the KEK radial-geometry source. The normalized emittances, within the 80% contour,

Table 12.6. Negative-ion beam currents (peak) produced by the high-intensity plasma-sputter negative-ion source developed at KEK [120, 121]

Ion(%)	Probe Material	Probe Voltage (V)	Cathode Geometry	Current (mA)
C^-(36)	C	937	Spherical	6.0
C_2^-(58)	C	937	Spherical	6.0
O^-(67)	Mo and O_2	438	Spherical	30
Si^-(75)	Si	937	Spherical	6.0
P^-(44)	GaP	937	Flat	1.8
Co^-(85)	Co	937	Spherical	6.0
Ni^-(87)	Ni	438	Spherical	6.0
Cu^-(77)	Cu	438	Spherical	8.2
Cu^-(40)	CuO	438	Flat	4.5
O^-(60)	CuO	438	Flat	4.5
As^-(20)	GaAs	937	Flat	3.7
As_2^-(52)	GaAs	937	Flat	3.7
Pd^-(69)	Pd	937	Spherical	7.6
Ag^-(91)	Ag	937	Spherical	6.2
Sn^-(67)	Sn	937	Spherical	3.6
Pt^-(71)	Pt	937	Spherical	8.1
Au^-(73)	Au	437	Spherical	10.3
Bi^-(6)	Bi	937	Spherical	2.7
O^-(42)	Bi	937	Spherical	2.7

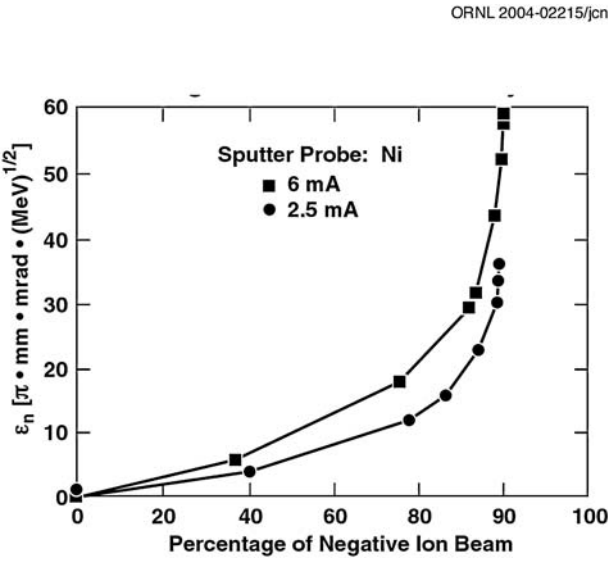

Fig. 12.30. Normalized emittances, within the 80% contour, for 2.5 mA and 6 mA Ni beams for the pulsed-mode high-intensity plasma-sputter negative-ion source [120, 121]

for 2.5 mA and 6 mA Ni beams are, respectively, $\sim 12\pi$ mm mrad $(\mathrm{MeV})^{1/2}$ and 17π mm mrad $(\mathrm{MeV})^{1/2}$, as shown in Fig. 12.30. The increase in emittance is attributable to space-charge effects in the beam. An axial-geometry version of this source has also been designed for pulsed-mode operation for potential use in tandem accelerator/heavy-ion synchrotron applications at the Oak Ridge National Laboratory [122].

The Kyoto University RF Plasma-Sputter Negative-Ion Source

A DC-mode plasma-sputter negative-ion source using a 13.56 MHz RF plasma igniter has been developed at Kyoto University in Japan [123, 124]. The source, shown schematically in Fig. 12.31, differs from previously described sources of this type in that it is not equipped with provision for plasma confinement. The source generates a high-density plasma from Ar or Xe gas seeded with Cs vapor by application of RF power to a three-turn antenna. The spherical-sector cathode ($\phi = 43$ mm) is positioned 70 mm from the ion exit aperture ($\phi = 13$ mm). Beam intensities of 6.5 mA of Cu^-, 1.6 mA of C^-, 2.3 mA of C_2^-, 3.8 mA of Si^-, 0.03 mA of B^- and 1.0 mA of B_2^- have been generated in the source. The efficiencies for forming several negative ions in the source are given in Table 12.7. The emittances of beams extracted from the source have not been measured, but for the same species, intensity and extraction parameters, they are expected to be comparable to the

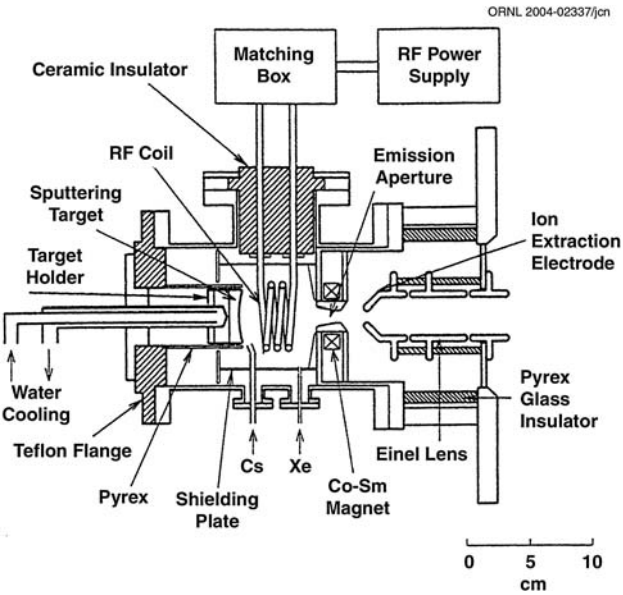

Fig. 12.31. A side view of the high-intensity RF plasma-sputter source developed at the University of Kyoto

Table 12.7. Maximum efficiencies for negative-ion production in the Kyoto University RF plasma-sputter negative-ion source

Ion	C^-	Si^-	Cu^-	Ge^-	Mo^-	Ta^-	W^-
Efficiency (%)	18.3	15.6	12.1	13.6	0.28	0.87	8.1

sources described in [120, 121] because of the similarities in physical size of their respective sputter cathodes and emission apertures.

The KEK/University of Tsukuba Compact Axial-Geometry Plasma-Sputter Negative-Ion Source

Negative-ion beams have an advantage over their positive-ion counterparts for SIMS analysis of insulating materials because they avoid the chronic charge-up problems present whenever positive-ion beams are used for this application. Mori et al. developed a compact, axial-geometry plasma-sputter negative-ion source with a 16 mm diameter cathode, operating in the DC mode with a LaB_6 cathode for plasma ignition, for such applications [125]. The source has been successfully employed by Yurimoto et al. for SIMS analyses of isotopic ratios in meteorites which intrinsically have insulating properties [126]. Beam intensities of 1.5 mA of Cu^- and 0.85 mA of Au^- have been extracted from the source and transmitted through a mass-

analysis system. The emittance of a Cu beam at the 90% contour has a value $\varepsilon_n \cong 6\pi$ mm mrad $(\mathrm{MeV})^{1/2}$.

12.8 Acknowledgments

The author is indebted to the Physics Division of the Oak Ridge National Laboratory for financial support. The author is also indebted to Dr. Yan Zhang for assisting in computing energy distributions induced in beams by the charge-exchange process, and to Dr. Yuan Liu for assisting in calculating the energy distributions of sputter-generated neutral and negative ions and for supplying the measured energy distribution for Ni beams for comparison with the Nörskov and Lundqvist theory.

References

1. H.S.W. Massey: *Negative Ions*, 3rd edn. (Cambridge University Press, London 1976)
2. B.M. Smirnov: *Negative Ions* (McGraw-Hill, New York 1982)
3. K.R. Lykke, K.K. Murray, W.C. Lineberger: Phys. Rev. A **43**, 6104 (1991)
4. H. Hotop, W.C. Lineberger: J. Phys. Chem. Ref. Data **14**, 731 (1985)
5. V. Bunge, C.F. Bunge: Phys. Rev. A **19**, 452 (1979)
6. G.D. Alton, R.N. Compton, D.J. Pegg: Phys. Rev. A **28**, 1405 (1983)
7. L.M. Blau, R. Novick, D. Weinflash: Phys. Rev. Lett. **24**, 1268 (1970)
8. R. Novick, D. Weinflash: Proc. Int. Conf. Precision Measurements and Fundamental Constants, eds. D. N. Langenberg and B. N. Taylor, Gaithersburg, MD, 1970, Natural Bureau of Standards Spec. Publication No. 343 (1971) p. 403
9. T.J. Kvale, G.D. Alton, R.N. Compton, D.J. Pegg, J.S. Thompson: Phys. Rev. Lett. **55**, 484 (1985)
10. D.M. Neumark, K.R. Lykke, T. Anderson, W.C. Lineberger: Phys. Rev. A **32**, 1890 (1985)
11. C. Blondel et al.: Phys. Rev. A **40**, 3698 (1989)
12. R. Trainham, G.D. Fletcher, D.J. Larson: J. Phys. B **20**, L777 (1987)
13. V.V. Petrunin, J.D. Voldstad, P. Balling, P. Kristensen, T. Andersen, H.K. Haugen: Phys. Rev. Lett. **76**, 744 (1996)
14. D.G. Leopold, W.C. Lineberger: J. Chem. Phys. **85**, 51 (1986)
15. J. Ho, K.M. Ervin, W.C. Lineberger: J. Chem. Phys. **93**, 6987 (1990)
16. T.M. Miller, A.E.S. Miller, W.C. Lineberger: Phys. Rev. A **33**, 3558 (1986)
17. H.H. Andersen, V.V. Petrunin, P. Kristensen, T. Andersen: Phys. Rev. A **42**, 3247 (1997)
18. V.V. Petrunin, J.D. Voldstad, P. Balling, P. Kristensen, T. Andersen, H.K. Haugen: Phys. Rev. Lett. **75**, 1911 (1995)
19. C.H. Greene: Phys. Rev. A **42**, 1405 (1990)
20. V.A. Dzuba, G.F. Gribakin: Phys. Rev. A **55**, 2443 (1997)
21. T.J. Kvale, R.N. Compton, G.D. Alton, J.S. Thompson, D.J. Pegg: Phys. Rev. Lett. **56**, 592 (1986)

22. R.D. Srivastava, O.M. Uy, M. Farber: Trans. Faraday Soc. **67**, 2941 (1971)
23. P.S. Drzaic, J. Marks, J.I. Brauman: In *Gas Phase Chemistry*, vol. 3, ed. M.T. Bowers (Academic Press, Orlando 1984) p. 167
24. K.M. Ervin, W.C. Lineberger: submitted to J. Chem. Phys.
25. R. Klein, R.P. McGinnis, S.R. Leone: Chem. Phys. Lett. **100**, 475 (1983)
26. K.J. Taylor, C.L. Pettiette, M.J. Craycraft, O. Chenovsky, R.E. Smalley: Chem. Phys. Lett. **152**, 347 (1988)
27. D.G. Leopold, K.K. Murray, T.M. Miller, W.C. Lineberger: unpublished data
28. A.E. Stevens, C.S. Fiegerle, W.C. Lineberger: J. Chem. Phys. **78**, 5420 (1983)
29. T. Anderson, K.R. Lykke, D.M. Neumark, W.C. Lineberger: J. Chem. Phys. **86**, 1858 (1987)
30. A.E.S. Miller, C.S. Fiegerle, W.C. Lineberger: J. Chem. Phys. **84**, 4127 (1986)
31. K.M. McHugh, J.G. Eaton, G.H. Lee, H.W. Sarkas, L.H. Kidder, J.T. Snodgrass, M.R. Manaa, K.H. Bowen: J. Chem. Phys. **91**, 3792 (1989)
32. D.G. Leopold et al.: J. Am. Chem. Soc. **108**, 179 (1986)
33. A.A. Viggiano, J.F. Paulson, F. Dale, M. Henchman, N.G. Adams, D. Smith: J. Chem. Phys. **89**, 2264 (1985)
34. M.K. Scheller, R.N. Compton, L.S. Cederbaum: Science **270**, 1160 (1995)
35. W.B. Herrmannsfeldt: SLAC Report No. 166 (1973)
36. J.C. Whitson, J. Smith, J.H. Whealton: J. Comp. Phys. **28**, 408 (1978)
37. J.H. Whealton, M.A. Bell, R.J. Raridon, K.E. Rothe, P.M. Ryan: J. Appl. Phys. **64**, 6210 (1988)
38. J.E. Boers: A digital computer code for the simulation of electron and ion beams on a PC, IEEE Cat. No. 93CH3334-0 (1993) 213. (PBGUNS is an electron/ion optics simulation code, developed by Thunderbird Simulations, Garland, TX, USA)
39. P. Spädtke: AXCEL-Gesellschaft für Schwerionen forshung (GSI), Interaktives Simulationsprogramm zur Berechnung von zwiedimensionalen Potentialverteilungen electrostatischer Anordnungen sowie von Ionbahnen in electrostatischen Feldern unter Berhcksichtigung der Raumladung, Gesellschaft für Schwerionen forshung (GSI)-Report 9 (1983)
40. R. Becker, W.B. Herrmannsfeldt: Rev. Sci. Instr. **63**, 2756 (1992)
41. G.D. Alton, H. Bilheux: Proc. 15th Int. Workshop on ECR Ion Sources, Jyväskylä, Finland, JYFL Research Report No. 4/2002 (2002) p. 169
42. T.R. Walsh: J. Nucl. Eng. C **4**, 53 (1962)
43. C.D. Moak, H.E. Banta, J.N. Thurston, J.W. Johnson, R.F. King: Rev. Sci. Instr. **30**, 694 (1959)
44. P. Lawrence et al.: Nucl. Instr. Meth. **32**, 357 (1965)
45. H.T. Richards, G.M. Klody: Proc. 2nd Int. Conf. on Ion Sources, Vienna (1972) p. 804
46. J. Aubert, G. Gautherin, C. Lejeune: Proc. 2nd Int. Conf. on Ion Sources, Vienna (1972) p. 797
47. R.P. Bastide, N.B. Brooks, A.B. Wittkower, P.H. Rose, K.H. Purser: IEEE Trans. Nucl. Sci. **NS-12**, 775 (1965)
48. E. Heinicke, K. Bethge, H. Baumann: Nucl. Instr. Meth. **58**, 125 (1968)
49. H. Smith, H.T. Richards: Bull. Am. Phys. Soc. **18**, 617 (1973)
50. H.S.W. Massey: Rep. Prog. Phys. **12**, 248 (1949)
51. J.B. Hasted: Proc. Roy. Soc. A **205**, 421 (1951); **212**, 235 (1952)
52. G.D. Alton, D.L. Haynes: Physics Division Progress Report for period ending September 30, 1994, Oak Ridge National Laboratory, ORNL-6916, pp. 1–39

53. B.J. Donnally, G. Thoeming: Phys. Rev. **159**, 87 (1967)
54. G.D. Alton, T.J. Kvale, R.N. Compton, D.J. Pegg, J.S. Thompson: Nucl. Instr. Meth. A **244**, 142 (1986)
55. J. Heinemeier, P. Hvelplund: Nucl. Instr. Meth. **148**, 425 (1975)
56. J. Heinemeier, P. Hvelplund: Nucl. Instr. Meth. **148**, 65 (1975)
57. R.H. McFarland, A.S. Schlachter, J.W. Stearns, B. Liu, R.E. Olson: Phys. Rev. A **26**, 775 (1982)
58. G.I. Dimov, G.V. Roslyakov: Instr. Expl. Tech. **17**, 658 (1974)
59. R.J. Girnius, C.J. Anderson, L.W. Anderson: Phys. Rev. A **16**, 2225 (1977)
60. B.A. D'Yachkov, V.I. Zinenko: Sov. Phys. – Tech. Phys. **16**, 305 (1971)
61. R.M. Ennis, Jr., D.E. Schechter, G. Thoeming, D.B. Schlafke, B.L. Donnally: IEEE Trans. Nucl. Sci. **NS-14**, 75 (1967)
62. R.J. Girnus, L.W. Anderson: Nucl. Instr. Meth. **137**, 373 (1976)
63. A.S. Schlachter, D.H. Loyd, P.J. Bjorkholm, L.W. Anderson, W. Haeberli: Phys. Rev. **171**, 20165 (1968)
64. J. Heinemeier, P. Hvelplund: unpublished
65. M. Kaminsky: *Atomic and Ionic Impact Phenomena on Metal Surfaces* (Springer, New York 1965)
66. H. Kawano, F.M. Page: Int. J. Mass. Spectr. Ion Phys. **50**, 1 (1983)
67. H. Kawano et al.: Int. J. Mass Spectr. Ion Phys. **50**, 35 (1983)
68. H. Kawano, Y. Hidaka, M. Suga, F.M. Page: Int. J. Mass Spectr. Ion Phys. **50**, 77 (1983)
69. J.M. Lafferty: J. Appl. Phys. **22**, 299 (1951)
70. V.S. Fomenko: *Emission Properties of Materials*, JPRS-56579 (NTIS, U.S. Dept. of Commerce, Springfield, VA 1972)
71. H. Ahmed, A.M. Broers: J. Appl. Phys. **43**, 185 (1972)
72. S. Hosoki, S. Yamamoto, K. Hayakawa, H. Okano: Jpn. J. Appl. Phys. (Suppl. 2, Part 1) 285 (1974)
73. H. Yamauchi, K. Takagi, I. Yuito, U. Kawabe: Appl. Phys. Lett. **29**, 638 (1976)
74. A. Avdienko, M.D. Malev: Vacuum **27**, 583 (1977)
75. G.D. Alton, M.T. Johnson, G.D. Mills: Nucl. Instr. Meth. A **328**, 154 (1993)
76. N. Kashihira, E. Vietske, G. Zellermann: Rev. Sci. Instr. **48**, 150 (1977)
77. B. Vosicki, T. Bornstad, L.C. Carraz, J. Heinemeier, H.L. Ravn: Nucl. Instr. Meth. **186**, 307 (1981)
78. G.D. Alton et al.: Nucl. Instr. Meth. B **211**, 425 (2003)
79. E. Krohn: J. Appl. Phys. **33**, 3523 (1962)
80. G.K. Wehner, G.S. Anderson: The nature of physical sputtering, in *Handbook of Thin Foil Technology*, Chapter 3, pp. 3-19, eds. L.I. Maissel and R. Glang (McGraw-Hill, New York 1970)
81. R. Behrisch, W. Heiland, W. Poschenrieder, P. Staib, H. Verbeek (eds.): *Ion Surface Interactions and Sputtering and related Phenomena* (Gordon and Breach, New York 1973)
82. H.H. Andersen, H.L. Bay: Sputtering yield measurements, in *Sputtering by Particle Bombardment* I, chapter 4, ed. R. Behrish, Topics in Applied Physics, Vol. 47 (Springer, New York 1981)
83. R. Behrish (ed.): *Sputtering by Particle Bombardment* II, Topics in Applied Physics, Vol. 52 (Springer, New York 1983)
84. M. Müller, G. Hortig: IEEE Trans. Nucl. Sci. **NS-16**, 3523 (1962)
85. G.D. Alton: IEEE Trans. Nucl. Sci. **NS-23**, No. 2, 1113 (1976)

86. R. Middleton, C.T. Adams: Nucl. Instr. Meth. **118**, 329 (1974)
87. G. Doucas, H.R.McK. Hyder, A.B. Knox: Oxford University report (1975)
88. K.R. Chapman: IEEE Trans. Nucl. Sci. **NS-23**, 1109 (1976)
89. G.D. Alton et al.: Nucl. Instr. Meth. B **170**, 515 (2000)
90. G.D. Alton, J.R. Beene: J. Phys. G, Nucl. Part. Phys. **24**, 1347 (1998)
91. G.D. Alton: Nucl. Instr. Meth. B **73**, 221 (1993)
92. G.D. Alton: Rev. Sci. Instr. **65**, 1141 (1994)
93. G.T. Caskey, R.A. Douglas, H.T. Richards, H.V. Smithe Jr.: Nucl. Instr. Meth. **157**, 1 (1978)
94. R. Middleton: Nucl. Instr. Meth. **214**, 139 (1983)
95. G.D. Alton: Nucl. Instr. Meth. A **244**, 133 (1986)
96. G.D. Alton, C.M. Jones: Nucl. Instr. Meth. A **244**, 170 (1986)
97. The Model 860 cesium-sputter negative-ion source is a product of the former General Ionex Corporation, Newburyport, MA, USA
98. G.D. Alton, G.D. Mills: IEEE Trans. Nucl. Sci. **NS-32**, 1822 (1985)
99. G.D. Alton, M.T. Johnson: Nucl. Instr. Meth. A **328**, 154 (1993)
100. I.D. Proctor: Nucl. Instr. Meth. B **40/41**, 727 (1989)
101. T.R. Niklaus, W. Baur, G. Bonani, M. Suter, H.A. Synal, W. Wöfli: Rev. Sci. Instr. **63**, 2485 (1992)
102. G. Du: Rev. Sci. Instr. **63**, 1151 (1992)
103. G.D. Alton: Proc. 11th Symposium on Ion Sources and Ion-Assisted Technology, Tokyo (1987) p. 157
104. G.D. Alton: *Proc. of the 1989 IEEE Particle Accelerator Conference*, 89CH2669-0, **Vol. 2**, 1112 (1989)
105. G.D. Alton, B. Cui, Y. Bao, C.A. Reed, J.A. Ball, C. Williams: Proc. 8th Inter. Conf. on Heavy Ion Accelerator Technology, American Institute of Physics (AIP) **CP473**, 352 (1999)
106. G.D. Alton, J.A. Benjamin: Nucl. Instr. Meth. **211**, 1 (1983)
107. G.D. Alton, G.D. Mills: Nucl. Instr. Meth. A **276**, 388 (1989)
108. R. Middleton: *A Negative Ion Cook Book* (1989) (unpublished)
109. G.D. Alton, J.W. McConnell, S. Tajima, G.J. Nelson: Nucl. Instr. Meth. B **24/25**, 826 (1987)
110. G.D. Alton, J.W. McConnell: Nucl. Instr. Meth. A **268**, 445 (1988)
111. H.H. Andersen, P. Tykesson: IEEE Trans. Nucl. Sci. **NS-22**, 1632 (1975)
112. P. Tykesson, H.H. Andersen, J. Heinemeier: IEEE Trans. Nucl. Sci. **NS-23**, 1104 (1976)
113. G.D. Alton, G.C. Blazey: Nucl. Instr. Meth. **166**, 105 (1979)
114. G.D. Alton, R.M. Beckers, J.W. Johnson: Nucl. Instr. Meth. A **244**, 146 (1986)
115. G.D. Alton, R. Lohwasser, B. Cui, Y. Bao, T. Zhang and C.A. Reed: Proc. 8th Inter. Conf. on Heavy Ion Accelerator Technology, American Institute of Physics (AIP) **CP473**, 340 (1999)
116. R.L. York and R.R. Stevens, Proc. 3rd International Conf. On Production and Neutralization of Negative Ion Beams, ed. K. Prelec, American Institute of Physics Conf. Proc. No. 111, New York, p. 410 (1984)
117. R.L. York, R.R. Stevens, Jr., R.A. DeHaven, J.R. McConnell, E.P. Chamberlain, R. Kandarian: Nucl. Instrum. and Meth. **B 10/11**, 891 (1985)
118. A. Takagi, Y. Mori, K. Ikegami, S. Fukumoto: IEEE Trans. Nucl. Sci. **NS-32** (5), 1782 (1985)

119. Y. Mori, A. Takagi, K. Ikegami, S. Fukumoto: Proc. 4th International Conf. On Production and Neutralization of Negative Ion Beams, ed. J.G. Alessi. (American Institute of Physics Conf. Proc. No. 158, New York, 1987) p. 378
120. G.D. Alton, Y. Mori, A. Takagi, A. Ueno, S. Fukumoto: Letters to the editor, Nucl. Instrum. and Meth. **A 270**, 194 (1988); ibid Nucl. Instrum. and Meth. **B 40/41**, 1008 (1989)
121. Y. Mori, G.D. Alton, A. Takagi, A. Ueno and S. Fukumoto, Nucl. Instrum. and Meth. **A 273**, 5 (1988)
122. G.D. Alton, Rev. Sci. Instrum. **63** 2455 (1992)
123. J. Ishikawa, H. Tsuji, Y. Okada, Y. Toyota, Y. Gotoh, Vacuum **44** 203 (1993)
124. H. Tsuji and J. Ishikawa, Rev. Sci. Instrum. **63**, 2488 (1992)
125. Y. Mori, Nucl. Instrum. and Meth., **A 328** 146 (1993)
126. H. Yurimoto, Y. Mori, and H. Yamamoto, Rev. Sci. Instr. **64** 1146 (1993)